C H A P T E R - VI

EXPERIMENTAL INVESTIGATIONS

6.1.0. GENERAL

As envisaged for the present research project various investigations in the realm of the shearing behaviour of jointed rock were conducted keeping in perspective the theoretical background developed in the previous chapter. Various factors were chosen so as to simulate the conditions as can be expected in certain physical situations. From the review on experimental investigations conducted concerning jointed rocks, it was inferred that the most trustworthy system would be the triaxial testing of laboratory prepared cylindrical specimens of jointed rocks. It has been recognized that servo controlled closed loop systems are superior than the conventional systems, however, in view of the simplicity and familiarity conventional systems are normally prefered. While the present work utilized the conventional system for the investigations to understand the influence of various aspects on shearing behaviour of jointed rocks, an effort, however, has been initiated to employ the most sophisticated recently perfected MTS System capable of testing the specimens under various complex stress fields.

6.2.0. TESTING SYSTEMS

6.2.1 Conventional triaxial test system

The conventional triaxial test setup is either stress controlled or strain controlled system. In stress controlled system the load is applied by dead weight through lever mechanism. The dead load system imparts step loading, hence response can not necessarily be instantaneous producing discontinuous response, further it is not possible to exactly identify the peak point and observe post peak behaviour, In view of this limitation of dead load system, the strain controlled mode of loading is prefered which enable to accomplish continuous response curve beyond peak point. However, the strain controlled system suffers from inadequacy as to the exact response since there is no feed back system incorporated in the conventional setup. The errors in the responses are due to the inherent inadequecies of measuring devices vis -a- vis the specimen, as for example the dilatancy measurement would be dependent on the stiffness of the proving ring and load frame, axialities of the displacement dial gauges and the degree of control for ambient pressures. The conventional test system is grossly inadequete for subjecting the specimen to programmed stress paths even under static loading condition while dynamic stress paths are not at all possible. For the present work a 10 tonne standard triaxial loading frame is employed. The driving machine consists of five pairs of driver and driven wheels and six levers, the combination of which produces thirty different speeds ranging from 4.83×10^{-5} cm/min. to 6.1×10^{-1} cm/min. A triaxial cell

used is 10 cms diameter perspex cell capable of withstanding 20 kg/cm^2 cell pressure and accomodate samples upto height of 20 cms. The strain rate used for the present investigation is 0.125 mm/min approximately 0.075 % per minute and confining pressures 2 kg/cm^2, 4 kg/cm^2 and 6 kg/cm^2 for cement sand samples and 2 kg/cm^2, 4 kg/cm^2, 6 kg/cm^2 and 8 kg/cm^2 for cement bentonite samples. The self compensating mercury control device is used for keeping cell pressure constant through out the test. The standard undrained compression tests were specified to be conducted under constant cell pressures. The failure occurs owing to increase in the major principal stress against constant minor and intermediate principal stresses. The load is measured with the help of proving rings of capacity 10 t and 5 t. The dial gauge of proving rings are calibrated and had proving ring constants 13.05 kg/div and 7.25 kg/div. respectively. The axial displacement of sample was measured with the help of Batty dial gauges having least count of 0.001 cm/div. and 0.0005 inch/div (0.00127 cm/div) respectively. The vertical displacement corresponding to load is noted at half a minute time interval.

Figure 6.1 shows a photograph of the conventional triaxial test setup.

6.2.2 Closed loop material testing system

In order to overcome the limitations of the conventional system, closed loop electro hydraulic servo controlled material testing system has been devised which is capable to simulate the demands of loading experienced by

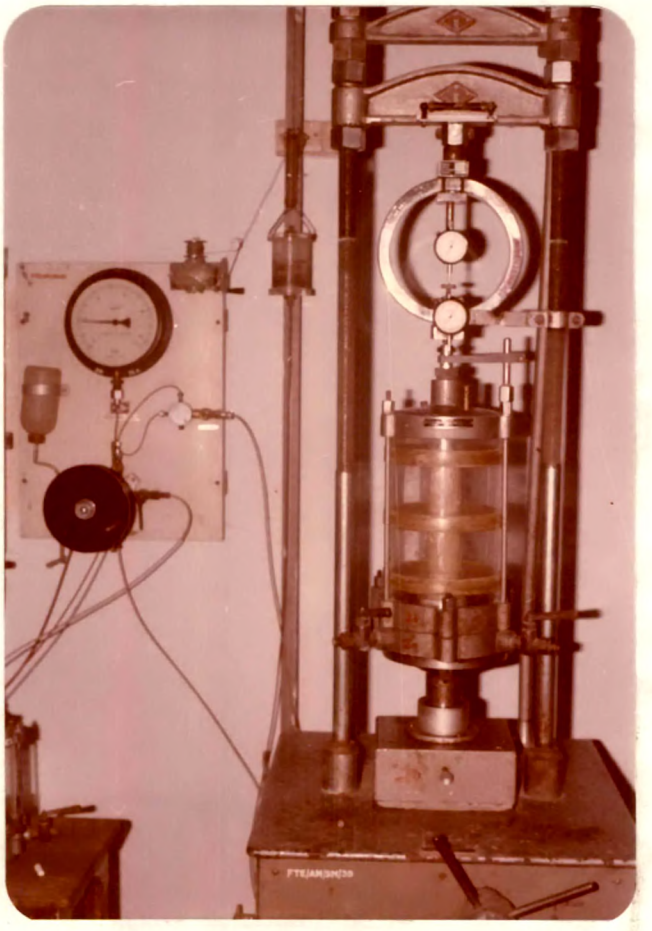

FIG. 6·1 TRIAXIAL TEST SET UP

the materials. The force, strain or displacement imposed on test specimen is measured and continuously compared in command input. The difference between the measured value and the command value is used to provide a continuous correction signal to the servo valve which causes this difference to be minimised. The transducer conditioners are used to excite the transducer and provide conditioning for the out put signal from the transducer which may be used for control and read out. Force, strain or displacement may be used as controlled parameters during the test. The system maintains the command value through out the test by continuously driving the servo value to provide the precisely controlled test in static and in dynamic conditions. The electronic signals with 0 to $\pm$ 10 Volt level provides a means for the utilization of numerous types of programming devices, recording devices and data processing and manipulation as required by the test.

The material testing system MTS Model 810 is used for the present work to test materials at loads upto 10 tons in tension or in compression, over an actuator stroke range of 150 mm. The triaxial cell includes complete porting, lines for pore fluids and is equipped with special bearing and seals for dynamic testing applications. The cell has capacity for confining pressures upto 20 kg/cm^2. The cell is also equipped with a sensitive displacement transducer to monitor specimen deformation. The MTS servo controller provides axial load or displacement control and control of confining pressure through de-intensifier. The programming of the system is achieved with the function generator. The

data recording display is consisting of a high speed strip chart recorder to record load, displacements and volume change. The load-displacement performance is recorded on the x-y plotter and also the printing of the same is done with the help of the dot matrix printer.

Fig. 6.2 shows a photograph of the servo controlled MTS Setup.

6.3.0. PREPARATION OF JOINTED SPECIMENS

6.3.1 General

During the present investigation few attempts were undertaken to produce jointed specimens in laboratory for the investigations envisaged. In order to apply the load on the desired sliding planes of the cubical sample an attempt was made to develop the grips to hold the sample in the desired planes of failure. These efforts were on the similar attempts undertaken at Imperial College of Science and Technology, London. In view of the difficulties encountered in applying loads on a cubical samples it was prefered to use core samples cut at the prefered joint orientation. An attempt was invested to produce a jointed rock in the laboratory simulating the field conditions by baking a joint in a furnace but it was rather a cumbersome process and therefore not considered worthwhile, therefore decided to follow the general procedure employed for preparing the jointed rock specimens normally used by research investigators.

6.3.2 Development of rock joint

To cut the specimen at desired orientations of 30°, 45° and 54.8° a set of special grips were developed as shown

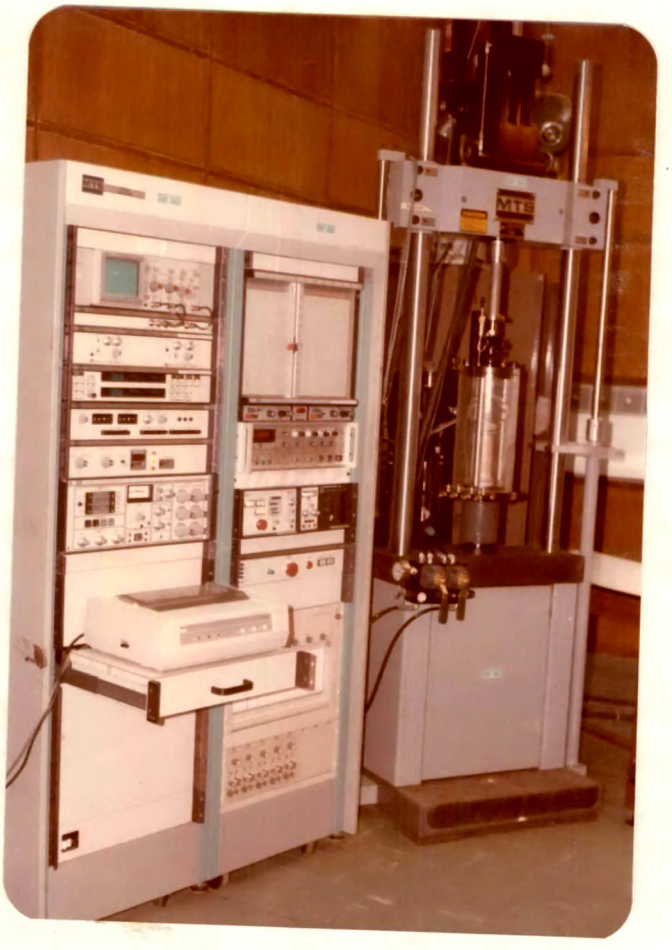

FIG. 6·2 MTS SET UP

in figure 6.3, 6.4 and 6.5. The samples were prepared in the following preportions of cement:bentonite, 50:50, 40:60 and 30:70 and cement : sand 1:2, 1:3 and 1:4 respectively. The procedure was to smear the paste of the gouge material to the desired thickness and after setting the samples were cleaned for extra paste adheard to sample near the joint. The sample thus prepared were checked for perfect cylindrical shape mainly for joint thickness by height gauge. These samples were cured in water upto full setting.

6.4.0. OBSERVATIONS

To investigate the influence of various aspects viz. joint orientation, gouge material characteristics and scale effect and to verify a failure criterion incorporating dilatancy parameter developed during the present investigation and to delineate the mechanism of failure of jointed rocks a series of experiments were planned during this project. As a part of this project a static event and a dynamic event were analysed to observe the shearing behaviour of a jointed rock. The observation recorded are presented in form of tables and plots. Various experiments are catagorized as below:

6.4.1 Category - I

Figure 6.6 to 6.14 represents graphical records of observations along with tables giving principal values of stress-strain at failure. Figures 6.6 to 6.8 show the stress-strain characteristic curves for specimens cut at 30°, 45° and 54.8° with the horizontal and filled with gouge material composed of cement : sand 1:2 and tested under cell

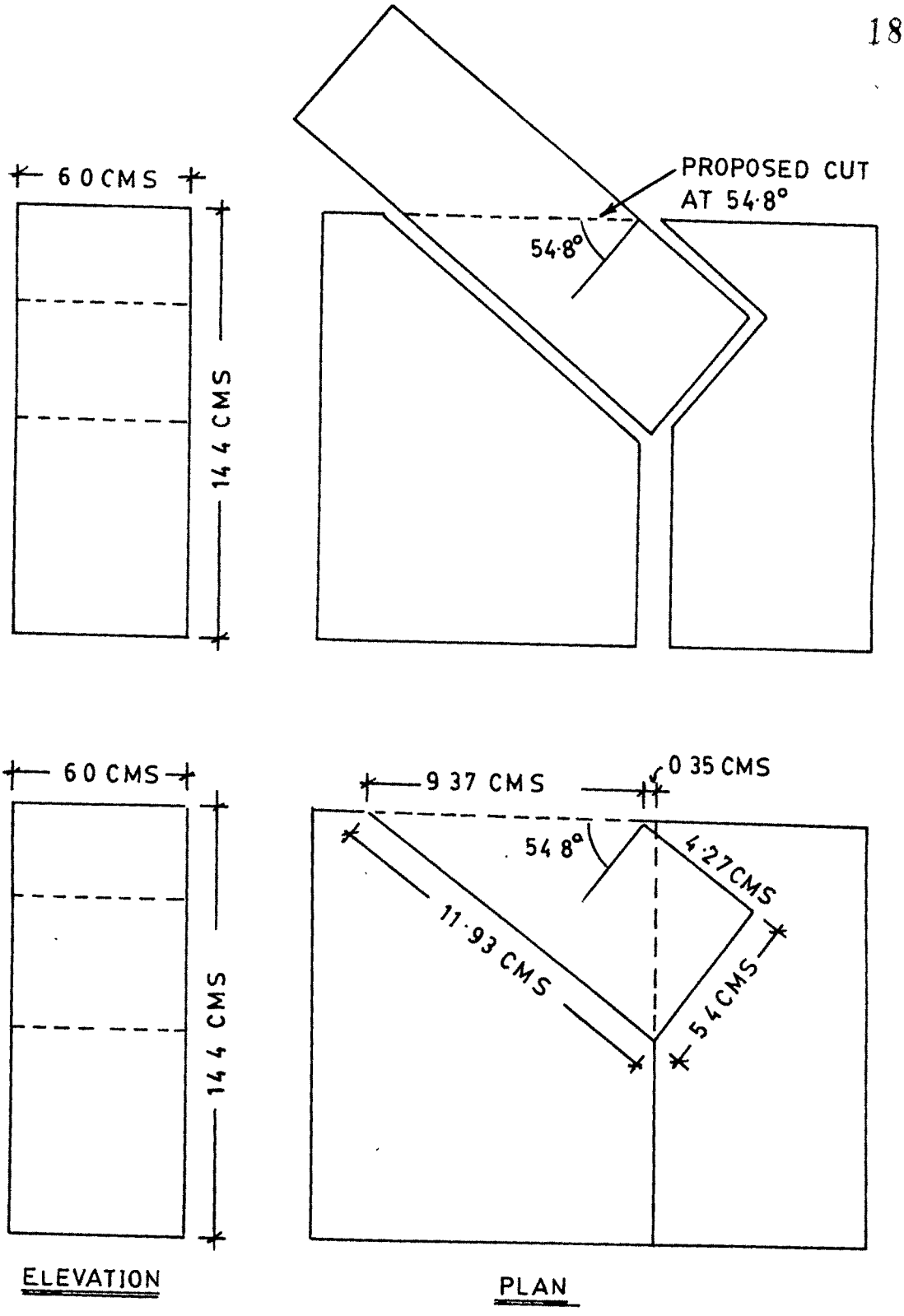

FIG.6-3 GRIP FOR ROCK CORE AT 54·8°. TWO SEPARATED PARTS SHOWN WITH ROCK CORE IN POSITION IN B

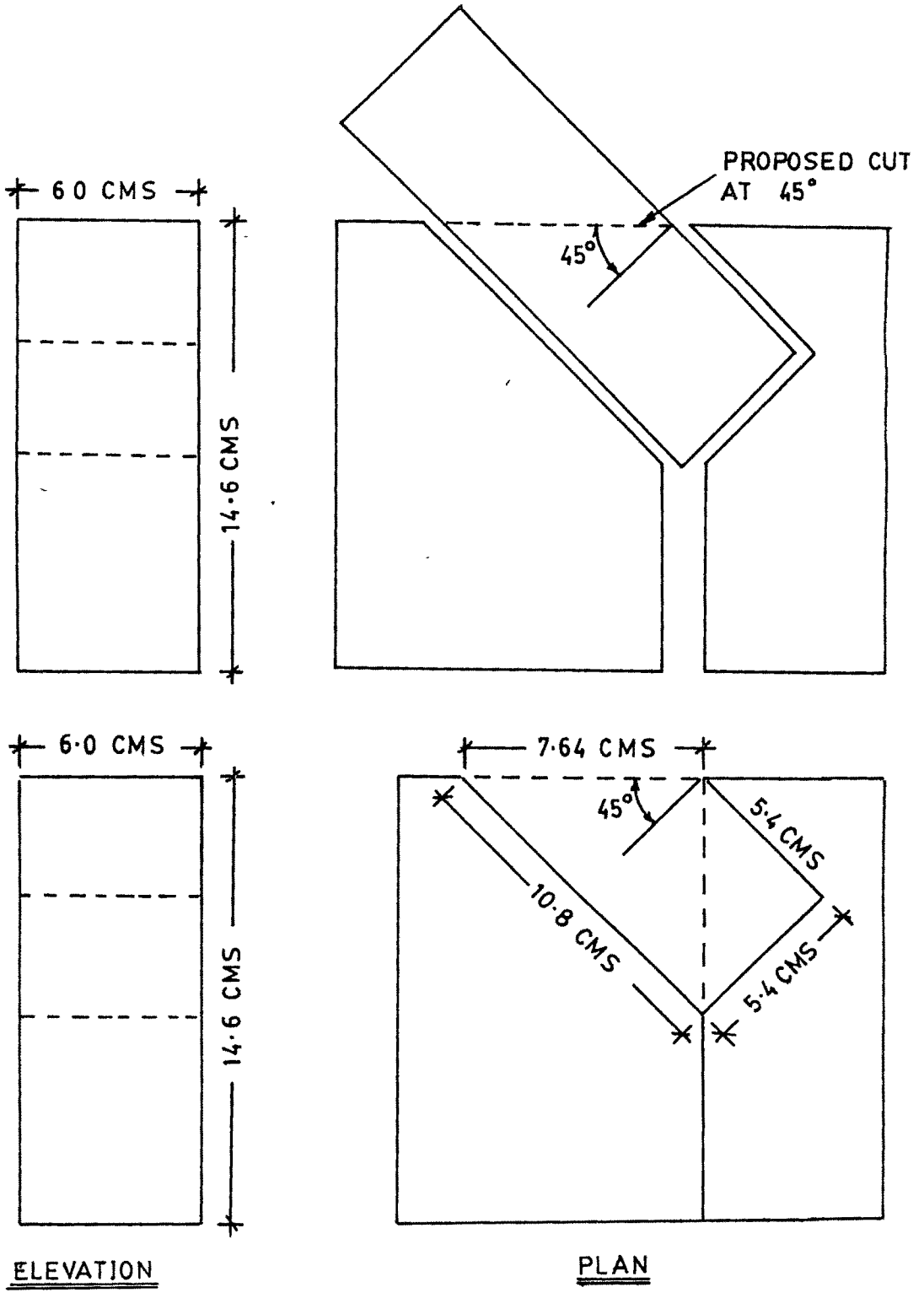

FIG.6·4 GRIP FOR ROCK CORE AT 45° TWO SEPARATED PARTS SHOWN WITH ROCK CORE IN POSITION IN B

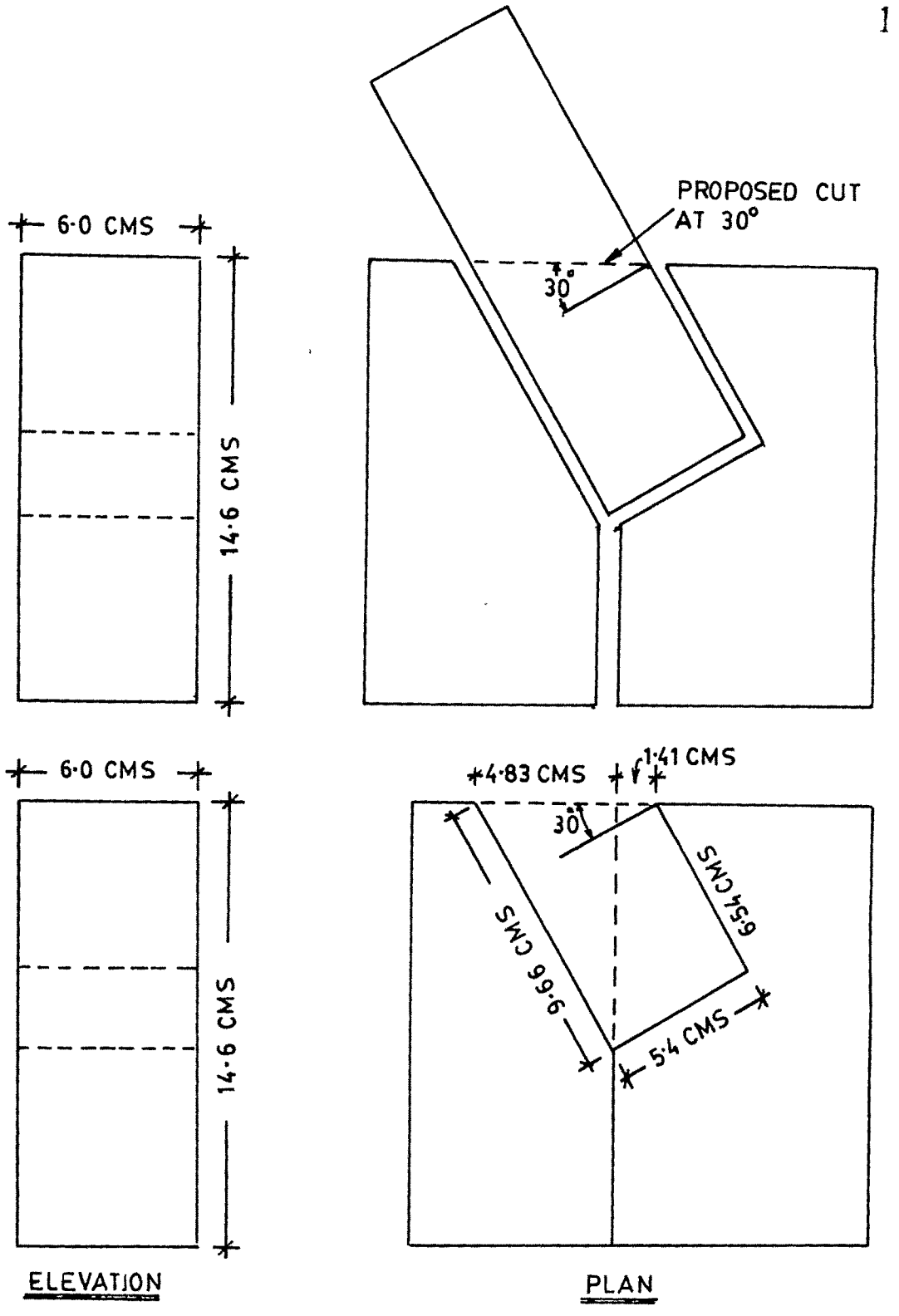

FIG.6·5 GRIP FOR ROCK CORE AT 30 TWO SEPARATED PARTS SHOWN WITH ROCK CORE IN POSITION IN B

190

	DESIGNATION	DEVIATOR STRESS AT FAILURE kg/cm²	STRESS RATIO AT FAILURE σ_1/σ_3	AXIAL STRAIN AT FAILURE 10^{-4}
———	$7/A_2^{30}$	84·84	43·43	170·40
- - - - -	$4/A_2^{45}$	71·57	36·78	135·80
— - —	$1/A_2^{54·8}$	53·68	27·84	91·00

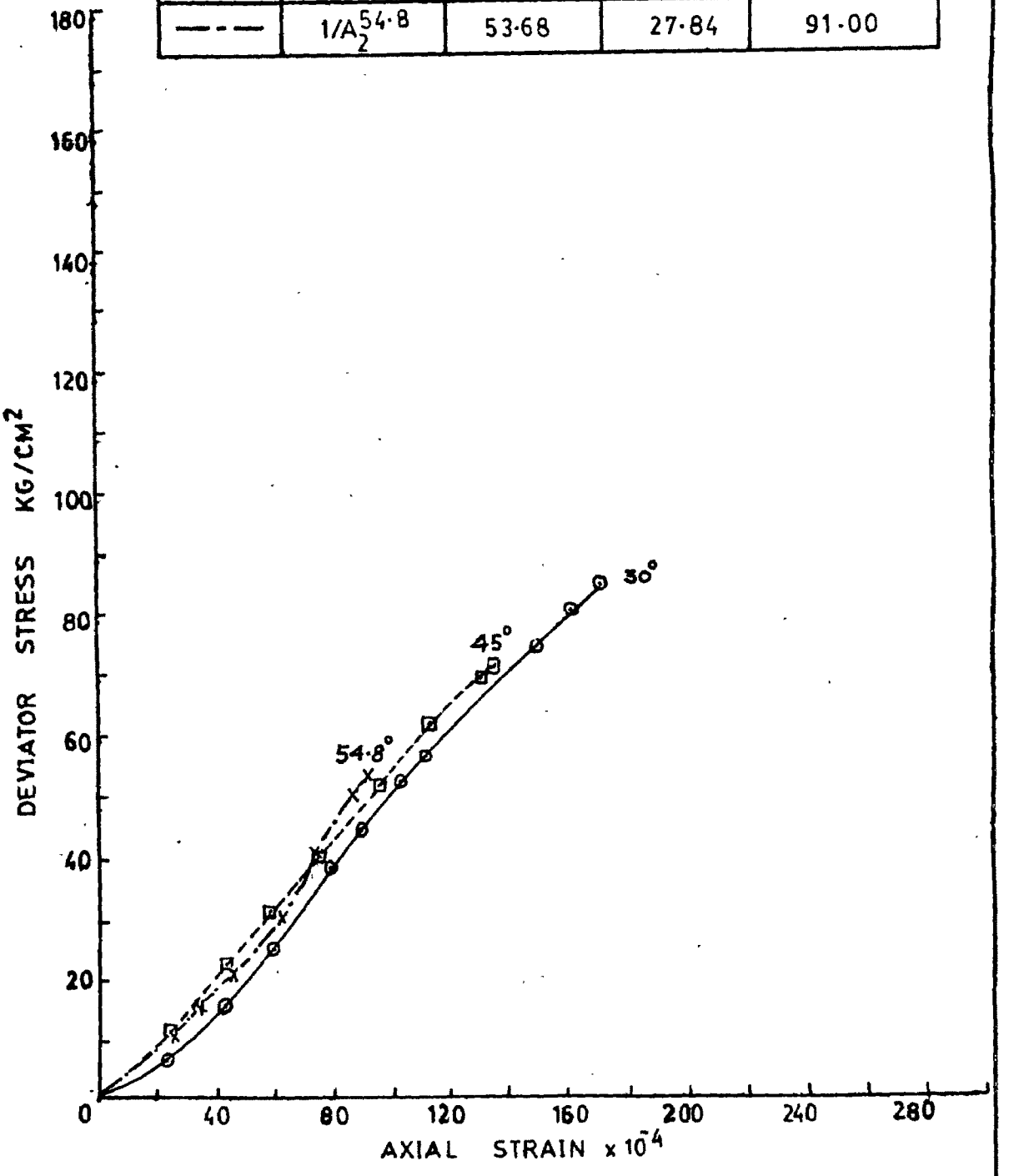

FIG 6·6 DEVIATOR STRESS AXIAL STRAIN CHARACTERISTIC CURVE

	DESIGNATION	DEVIATOR STRESS AT FAILURE kg/cm²	STRESS RATIO AT FAILURE σ_1/σ_3	AXIAL STRAIN AT FAILURE 10^{-4}
———	$8/A_4^{30}$	188·81	48·20	106·10
- - - - -	$5/A_4^{45}$	73·30	19·33	55·48
— - —	$2/A_4^{54·8}$	55·53	14·88	33 00

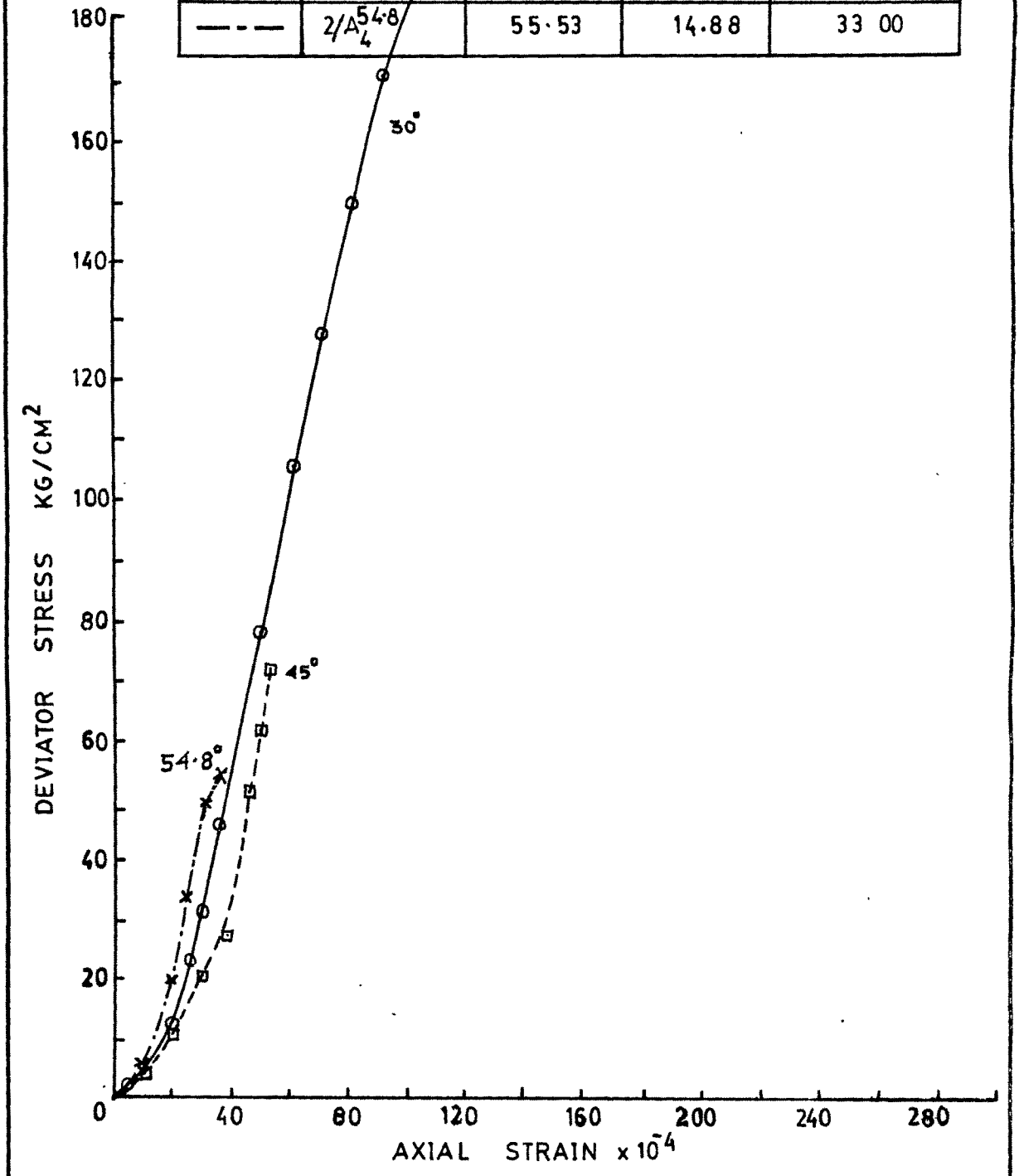

FIG 6·7 DEVIATOR STRESS AXIAL STRAIN CHARACTERISTIC CURVE

	DESIGNATION	DEVIATOR STRESS AT FAILURE Kg/cm²	STRESS RATIO AT FAILURE σ_1/σ_3	AXIAL STRAIN AT FAILURE 10^{-4}
———	$7/A_6^{30}$	277·61	141·83	200·00
- - - - -	$6/A_6^{45}$	76·08	13·60	45·73
—·—	$3/A_6^{54·8}$	63·86	11·64	50·61

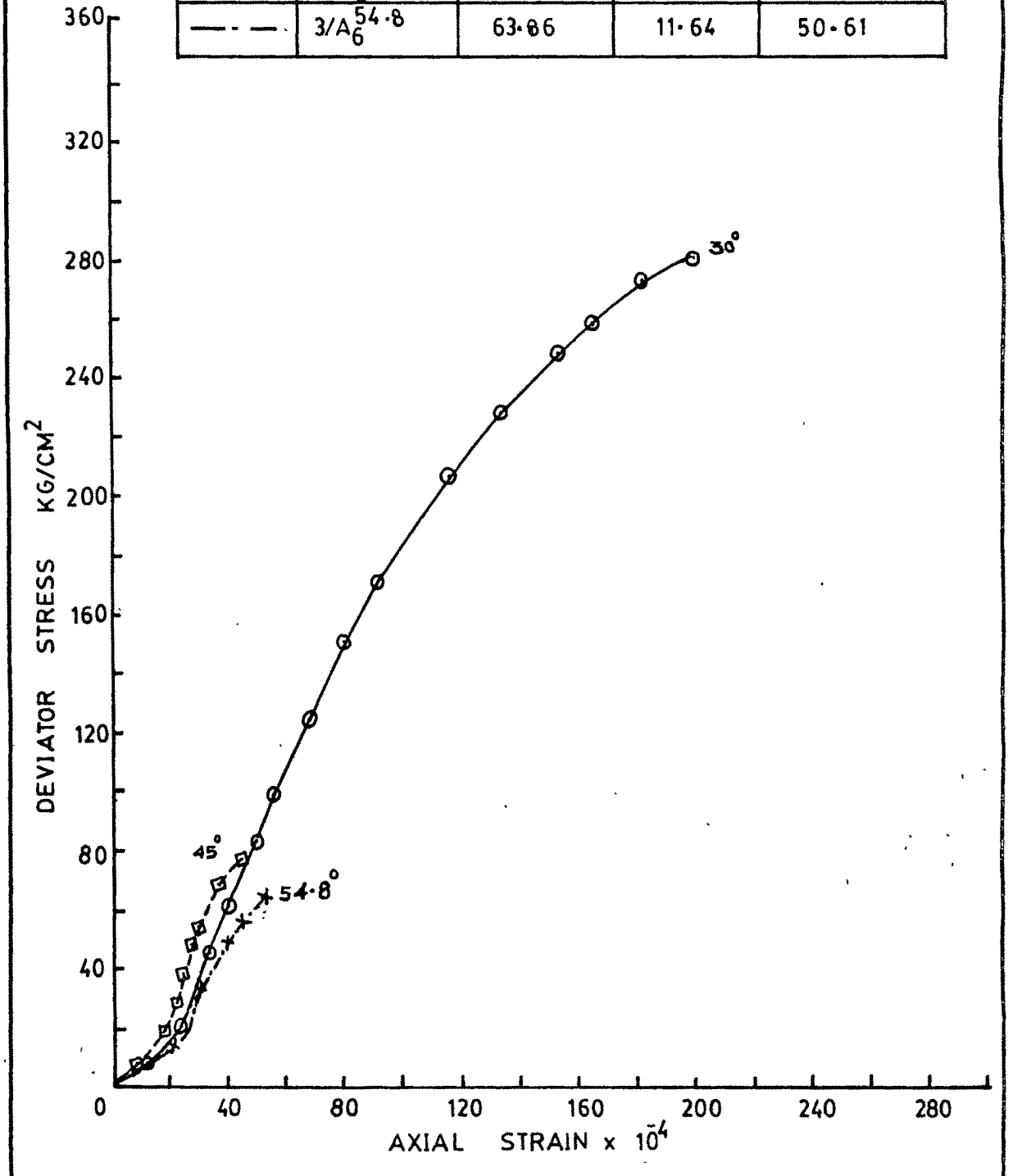

FIG 6·8 DEVIATOR STRESS AXIAL STRAIN CHARACTERISTIC CURVE

	DESIGNATION	DEVIATOR STRESS AT FAILURE kg/cm²	STRESS RATIO AT FAILURE σ_1/σ_3	AXIAL STRAIN AT FAILURE 10^{-4}
———	$16/B_2^{30}$	43·50	22·75	121·56
- - - - -	$13/B_2^{45}$	29·62	15·81	81·1
—·—·—	$10/B_2^{54\text{-}8}$	30·23	16·12	65·2

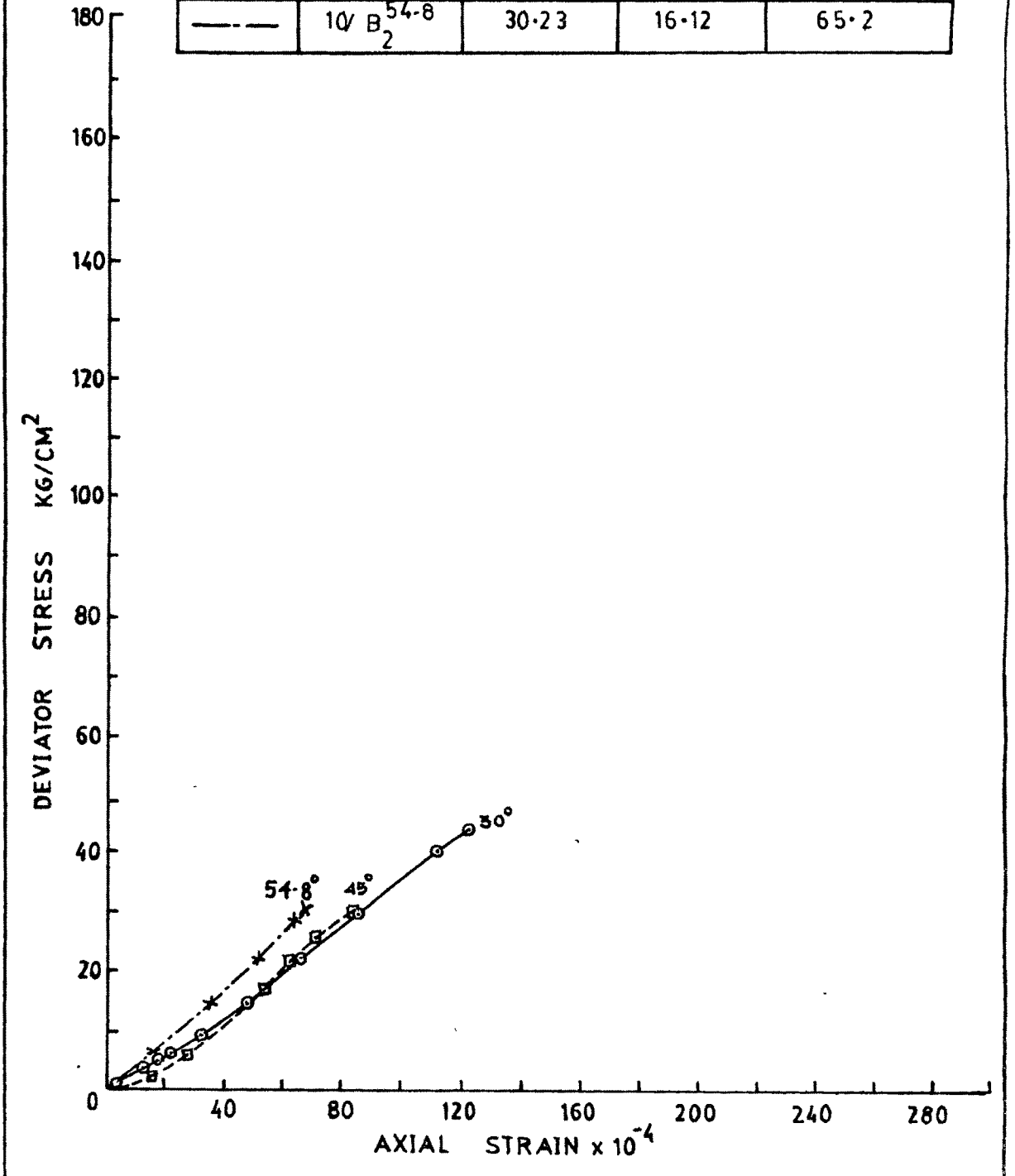

FIG. 6·9 DEVIATOR STRESS AXIAL STRAIN CHARACTERISTIC CURVE

	DESIGNATION	DEVIATOR STRESS AT FAILURE kg/cm²	STRESS RATIO AT FAILURE σ_1/σ_3	AXIAL STRAIN AT FAILURE 10^{-4}
———	$17/B_4^{30}$	90·70	23·68	171·00
- - - - -	$14/B_4^{45}$	33·14	9·50	69·40
—·—	$11/B_4^{54·8}$	30·85	8·71	118·00

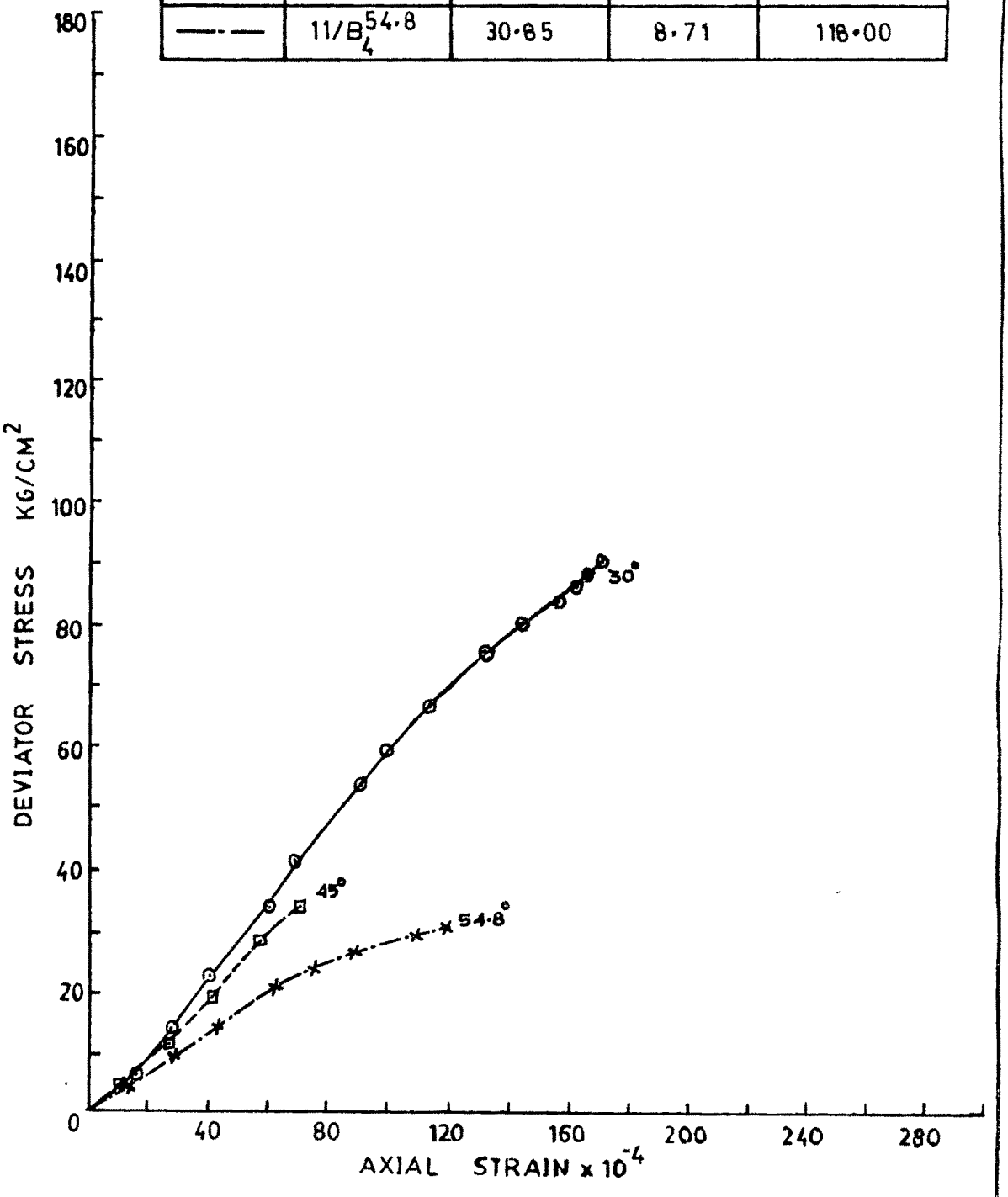

FIG. 6·10 DEVIATOR STRESS AXIAL STRAIN CHARACTERISTIC CURVE

	DESIGNATION	DEVIATOR STRESS AT FAILURE kg/cm²	STRESS RATIO AT FAILURE σ_1/σ_3	AXIAL STRAIN AT FAILURE 10^{-4}
———	$18/B_6^{30}$	112·17	19·70	64·24
- - - - -	$15/B_6^{45}$	56·64	10·44	23·17
—·—	$12/B_6^{54·8}$	52·76	9·79	27·44

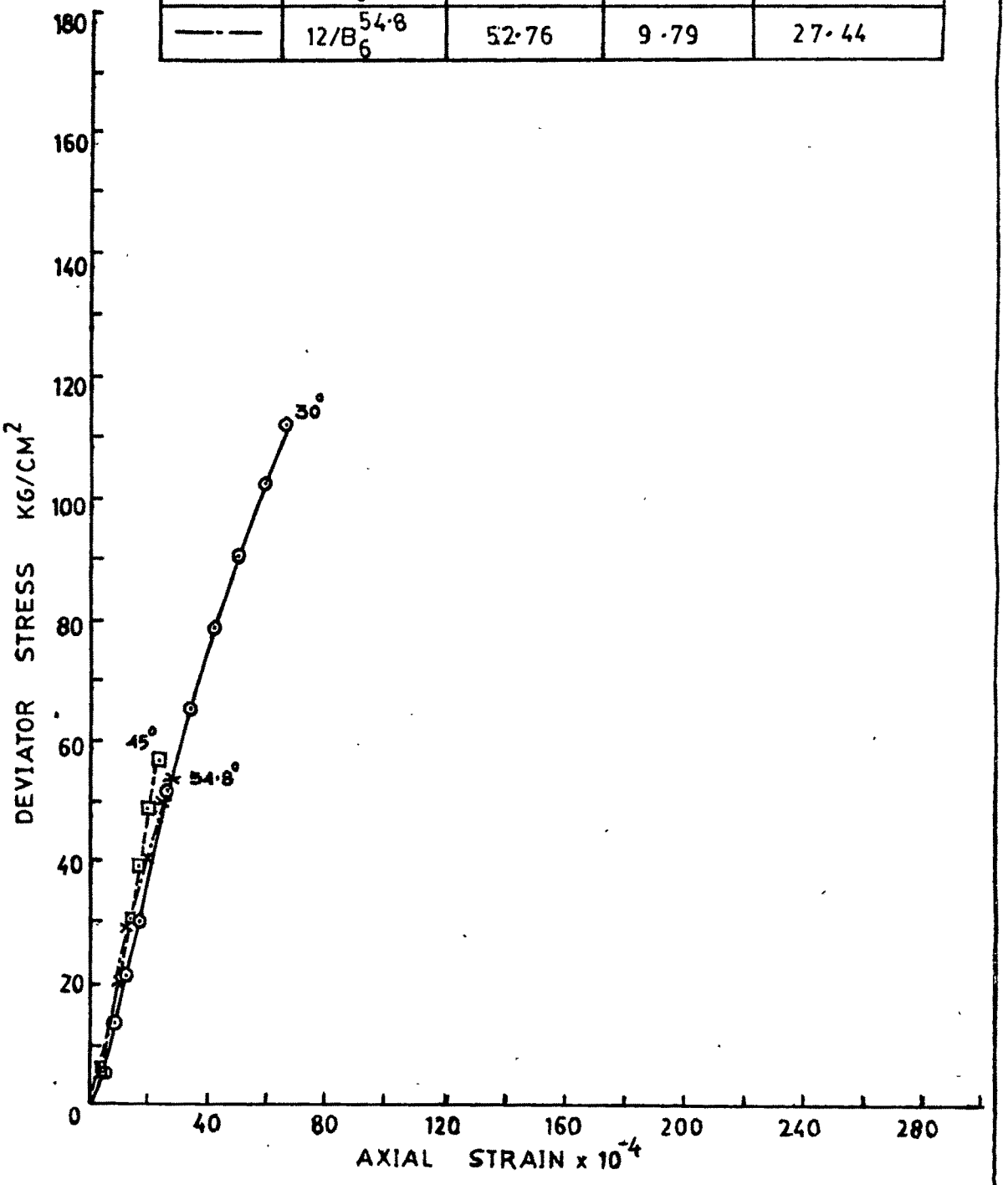

FIG. 6·11 DEVIATOR STRESS AXIAL STRAIN CHARACTERISTIC CURVE

	DESIGNATION	DEVIATOR STRESS AT FAILURE kg/cm²	STRESS RATIO AT FAILURE σ_1/σ_3	AXIAL STRAIN AT FAILURE 10^{-4}
———	$25/C_2^{30}$	80·21	41·11	128·74
- - - - -	$22/C_2^{45}$	20·67	11·34	42·0
—·—	$19/C_2^{54·8}$	14·81	8·41	31·7

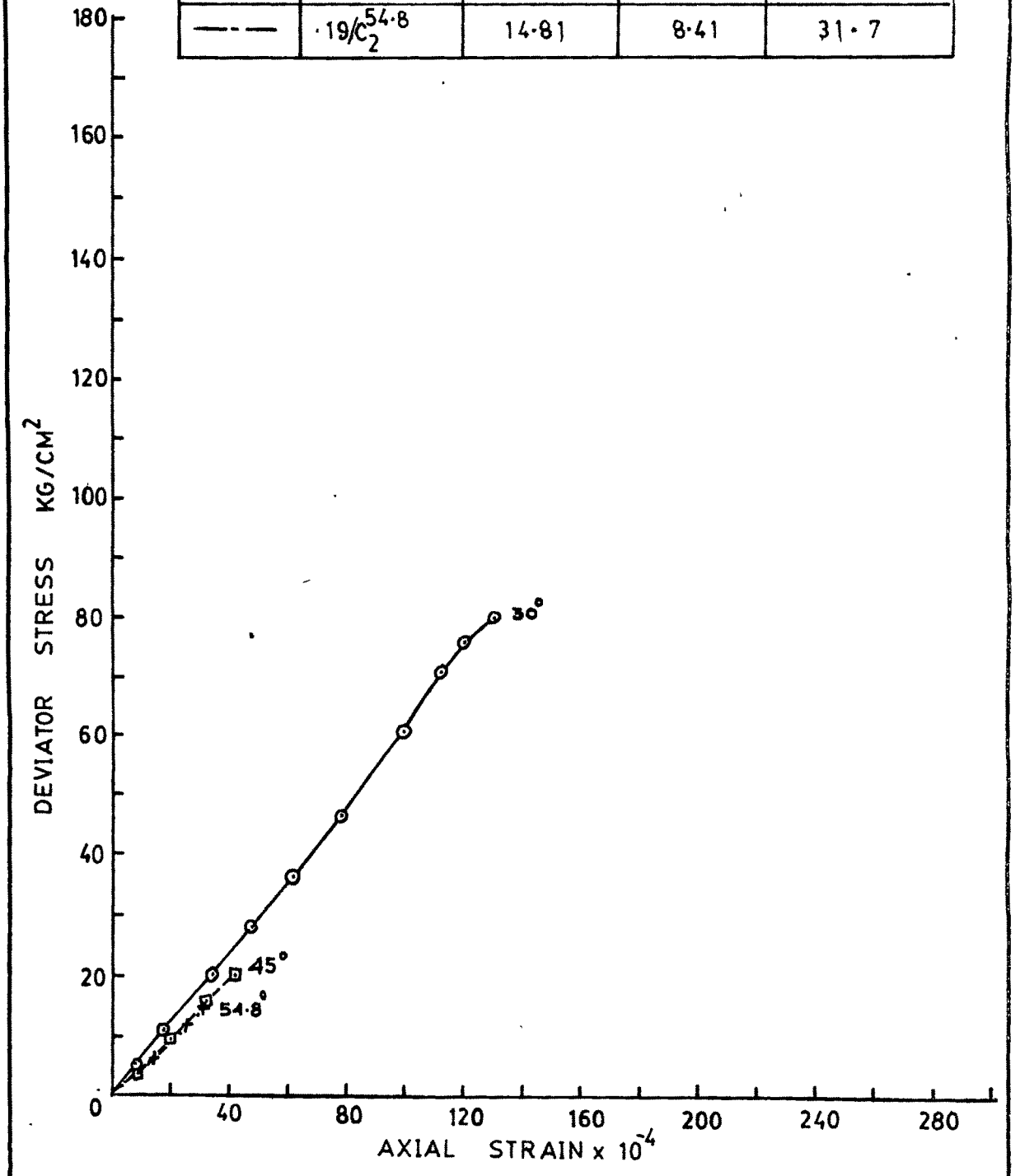

FIG.6·12 DEVIATOR STRESS AXIAL STRAIN CHARACTERISTIC CURVE

	DESIGNATION	DEVIATOR STRESS AT FAILURE kg/cm²	STRESS RATIO AT FAILURE σ_1/σ_3	AXIAL STRAIN AT FAILURE 10^{-4}
———	$26/C_4^{30}$	83·60	21·90	163·06
- - - - -	$23/C_4^{45}$	26·22	7·56	69·51
—·—	$20/C_4^{54\cdot8}$	21·90	6·48	52·9

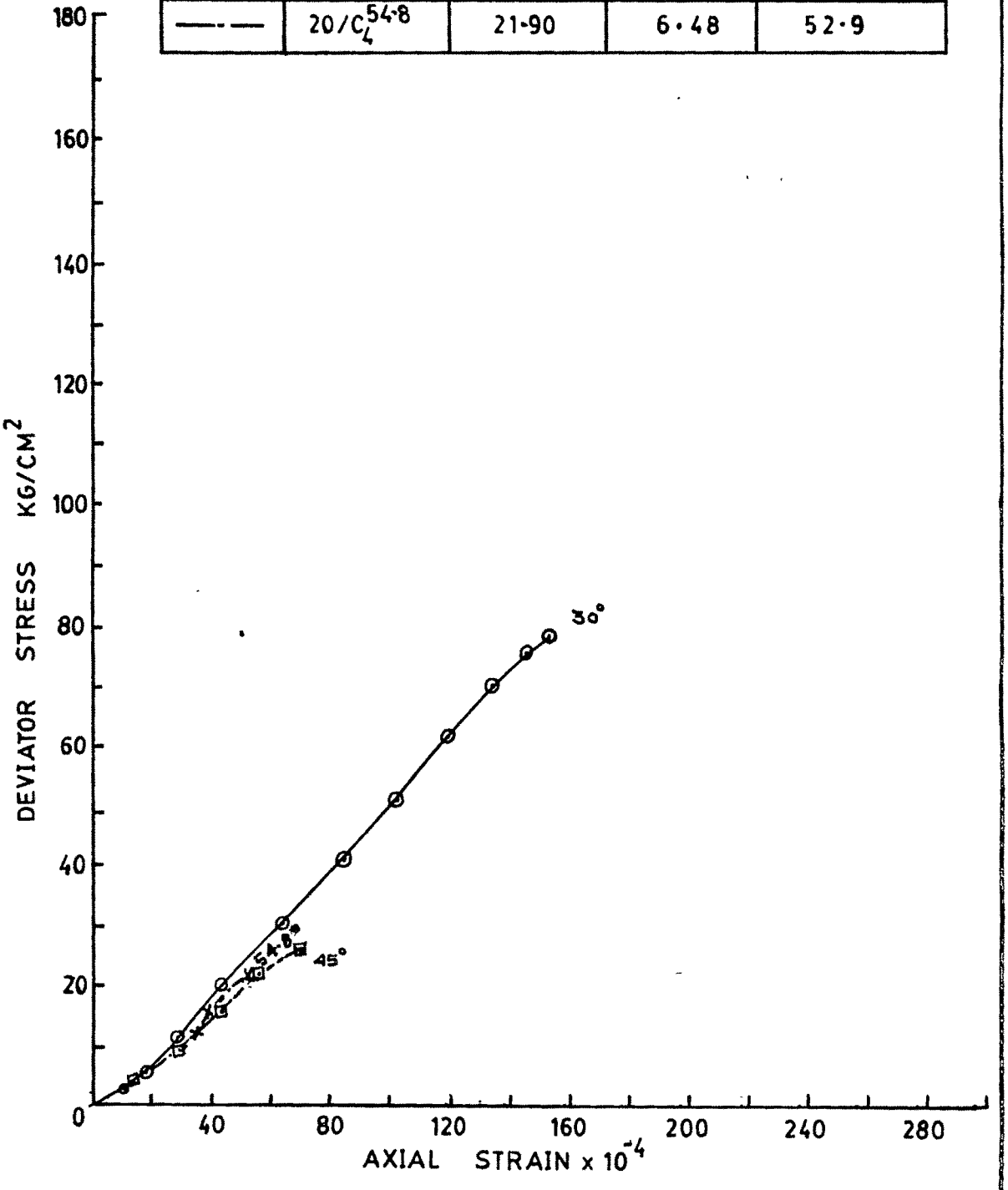

FIG.6·13 DEVIATOR STRESS AXIAL STRAIN CHARACTERISTIC CURVE

	DESIGNATION	DEVIATOR STRESS AT FAILURE kg/cm^2	STRESS RATIO AT FAILURE σ_1/σ_3	AXIAL STRAIN AT FAILURE 10^{-4}
———	$27/C_6^{30}$	29·43	5·91	28·00
- - - - -	$24/C_6^{45}$	30·54	6·09	22·48
—·—	$21/C_6^{54·8}$	29·43	5·91	26·34

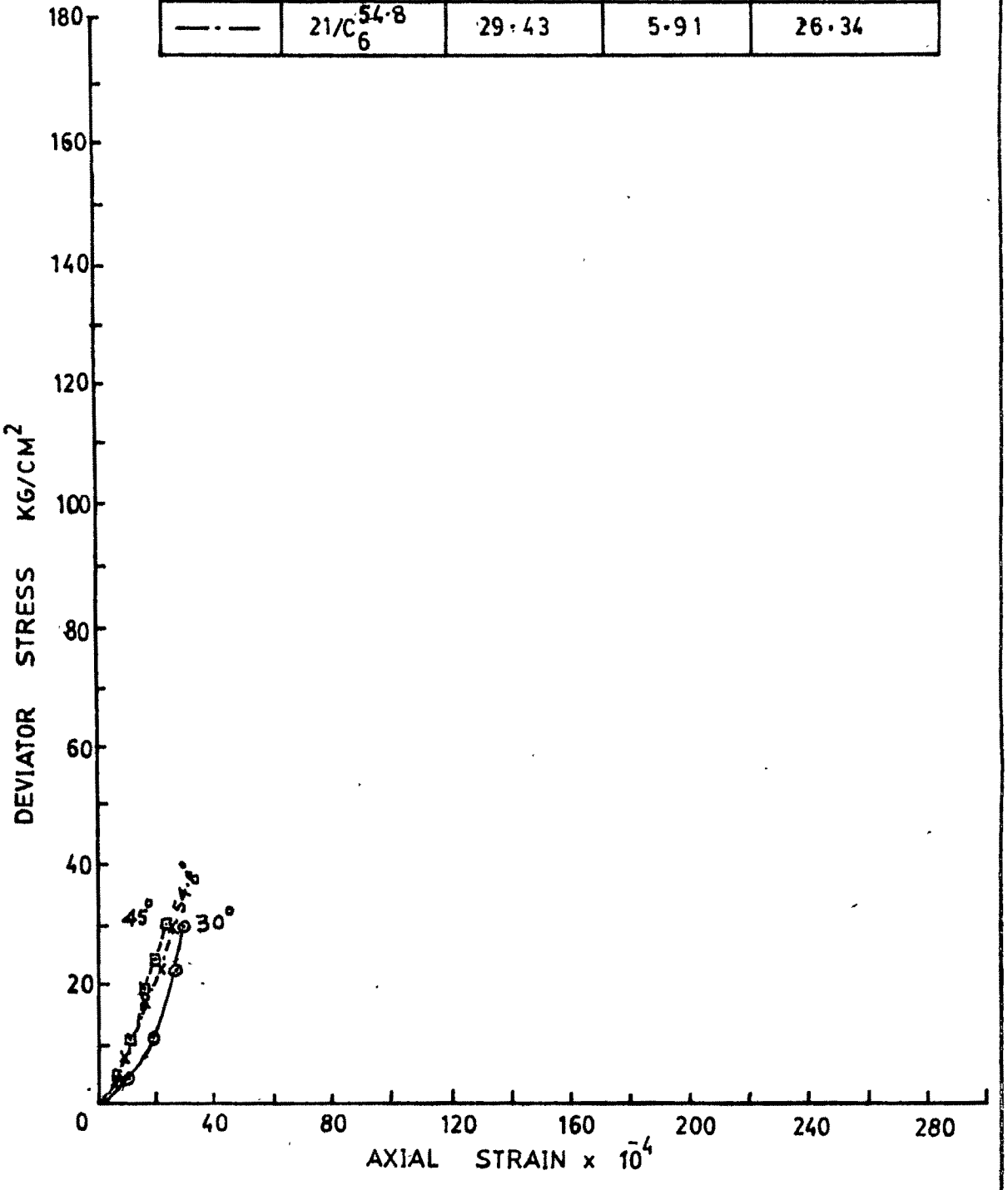

FIG.6·14 DEVIATOR STRESS AXIAL STRAIN CHARACTERISTIC CURVE

pressures 2 kg/cm^2, 4 kg/cm^2 and 6 kg/cm^2. Figures 6.9 to 6.11 and 6.12 to 6.14 are similar presentations for gouge material cement : sand 1:3 and 1:4 respectively. Just near the peak stress a sudden sliding associated with a characteristic thud noise was noticed in most of the specimens. The failure was so instantaneous that it was impossible to observe the post peak stress-strain readings. The nature of most of the stress-strain curves is typical with a concave downward in the early stages while slight concave upward just near the peak. In other wards modulii are varying throughout the process of deformation. The effect is predominantly seen for the specimens with 30° joint orientations, 6 kg/cm^2 cell pressure and 1:2 gouge material (Fig. 6.8). For 30° joint orientation principal values namely peak stress, maximum stress ratio, and strain at peak stress shows a good degree of upward variation in comparision with joint orientation 45° and 54.8°.

6.4.2 Category - II

Figures 6.15 to 6.31 represent graphically along with tables the principal values of stress and strain at failure. Figures 6.15 to 6.17 portrays the stress-strain curve of specimens possessing gouge materials cement:sand 1:2 1:3 and 1:4 at 54.8° joint orientation and tesed under cell pressure 2 kg/cm^2, 4 kg/cm^2 or 6 kg/cm^2. Fig. 6.18 to 6.20 and 6.21 to 6.23 are similar presentations for the joint orientations 45° and 30° respectively. Also figure 6.24 to 6.27 show the stress-strain curves for the specimens filled with gouge materials cement:bentonite 50:50, 40:60 and

200

	DESIGNATION	DEVIATOR STRESS AT FAILURE kg/cm²	STRESS RATIO AT FAILURE σ_1/σ_3	AXIAL STRAIN AT FAILURE 10^{-4}
———	$2/A_4^{54.8}$	55.53	14.88	33.00
- - - - -	$11/B_4^{54.8}$	30.85	8.71	118.00
—·—	$20/C_4^{54.8}$	21.90	6.48	52.90

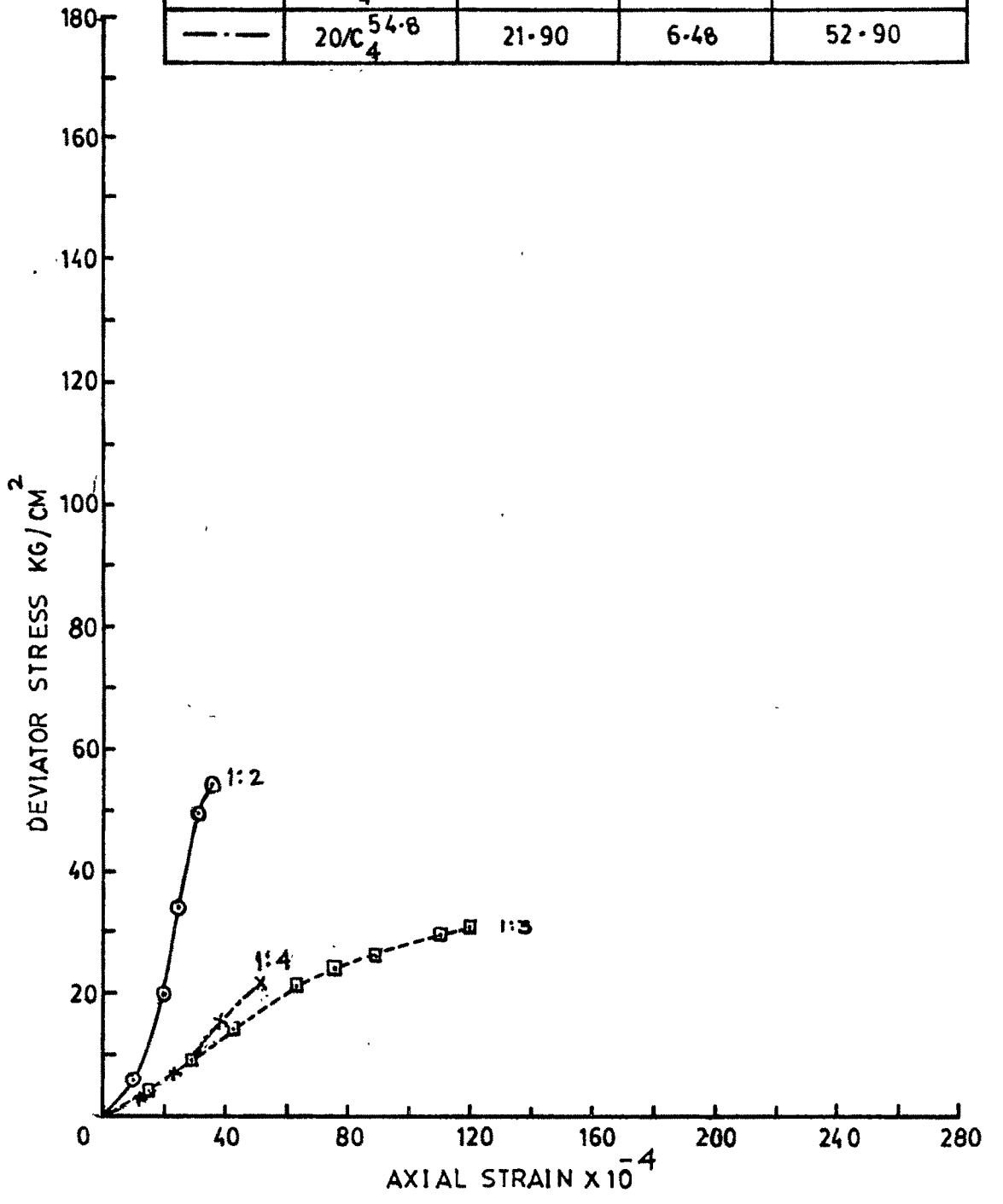

FIG.6·16 DEVIATOR STRESS AXIALSTRAIN CHARACTERISTIC CURVE

	DESIGNATION	DEVIATOR STRESS AT FAILURE kg/cm²	STRESS RATIO AT FAILURE σ_1/σ_3	AXIAL STRAIN AT FAILURE 10^{-4}
———	$2/A_4^{54.8}$	55.53	14.88	33.00
- - - - -	$11/B_4^{54.8}$	30.85	8.71	118.00
—·—	$20/C_4^{54.8}$	21.90	6.48	52.90

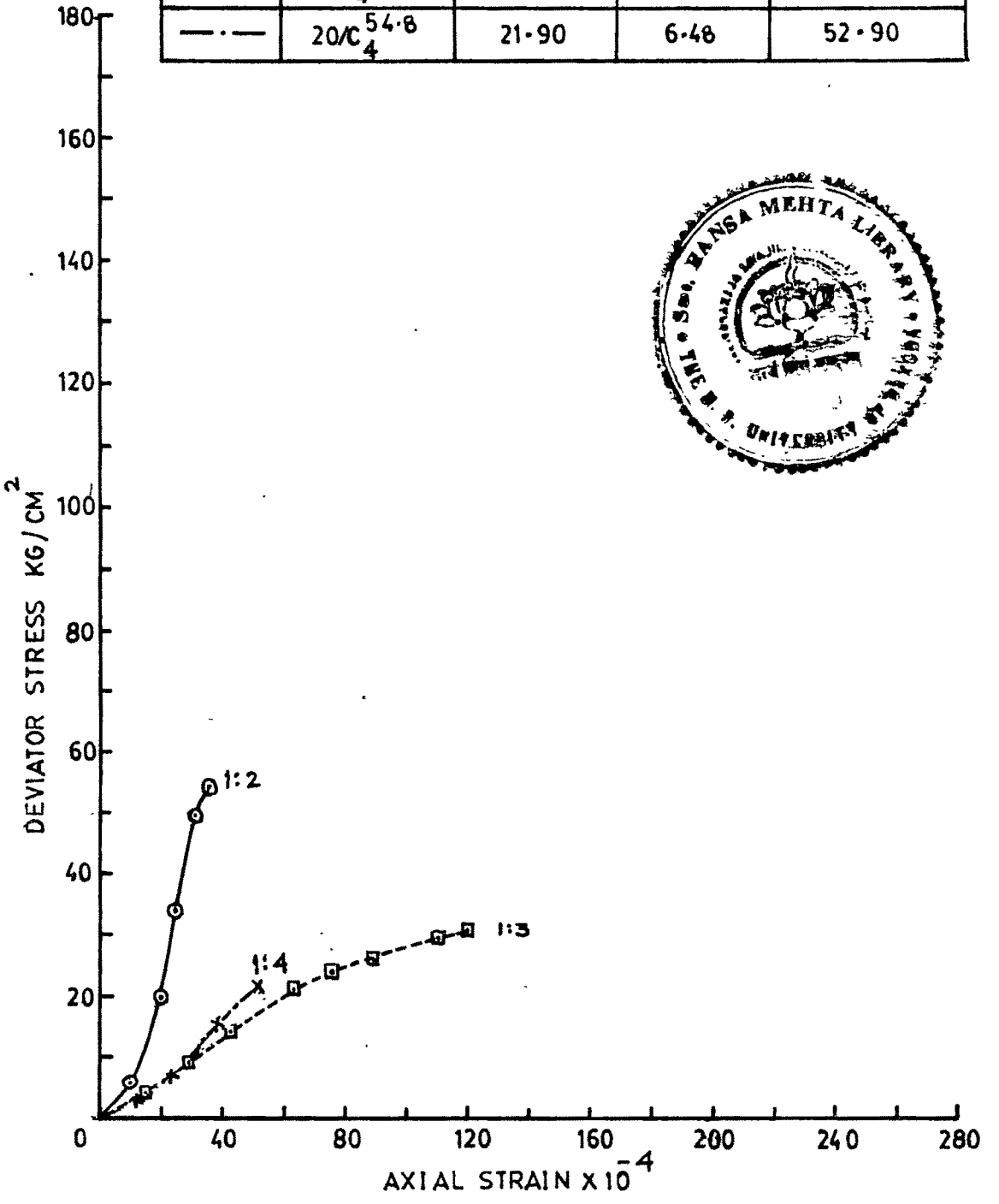

FIG.6-16 DEVIATOR STRESS AXIALSTRAIN CHARACTERISTIC CURVE

	DESIGNATION	DEVIATOR STRESS AT FAILURE kg/cm²	STRESS RATIO AT FAILURE σ_1/σ_3	AXIAL STRAIN AT FAILURE 10^{-4}
———	$3/A_6^{54.8}$	63·86	11·64	50·61
- - - - -	$12/B_6^{54.8}$	52·76	9·79	27·44
—·—	$21/C_6^{54.8}$	29·43	5·91	26·34

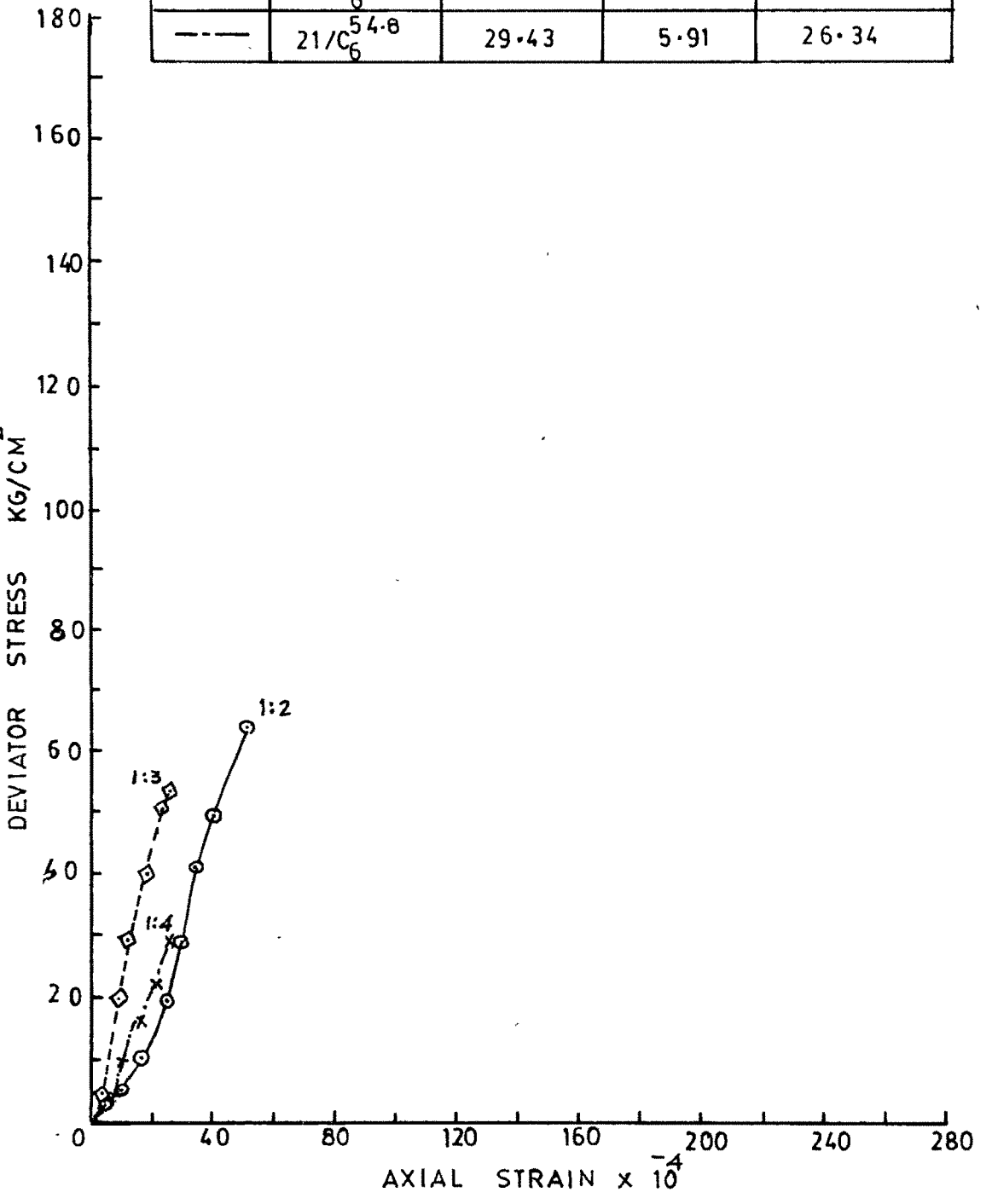

FIG.6·17 DEVIATOR STRESS AXIAL STRAIN CHARACTERSTIC CURVE

	DESIGNATION	DEVIATOR STRESS AT FAILURE kg/cm²	STRESS RATIO AT FAILURE σ_1/σ_3	AXIAL STRAIN AT FAILURE 10^{-4}
———	$4/A_2^{45}$	71·57	36·78	135·80
- - - - -	$13/B_2^{45}$	29·62	15·81	81·10
—·—	$22/C_2^{45}$	20·67	11·34	42·00

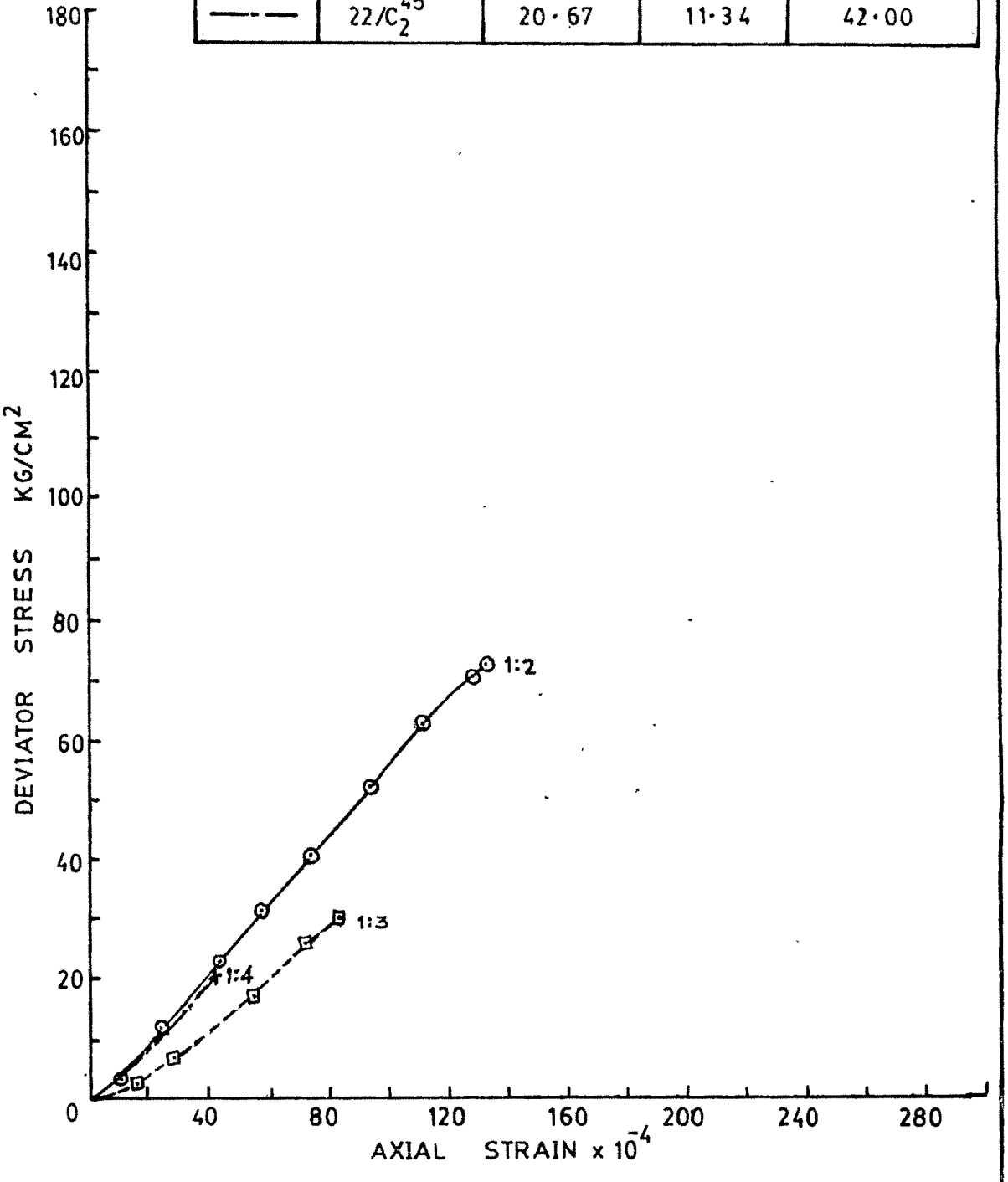

FIG. 6·18 DEVIATOR STRESS AXIAL STRAIN CHARACTERISTIC CURVE

	DESIGNATION	DEVIATOR STRESS AT FAILURE kg/cm^2	STRESS RATIO AT FAILURE σ_1/σ_3	AXIAL STRAIN AT FAILURE 10^{-4}
———	$5/A_4^{45}$	73·30	19·33	55·48
- - - - -	$14/B_4^{45}$	33·74	9·50	69·40
—·—	$23/C_4^{45}$	21·90	6·48	52·9

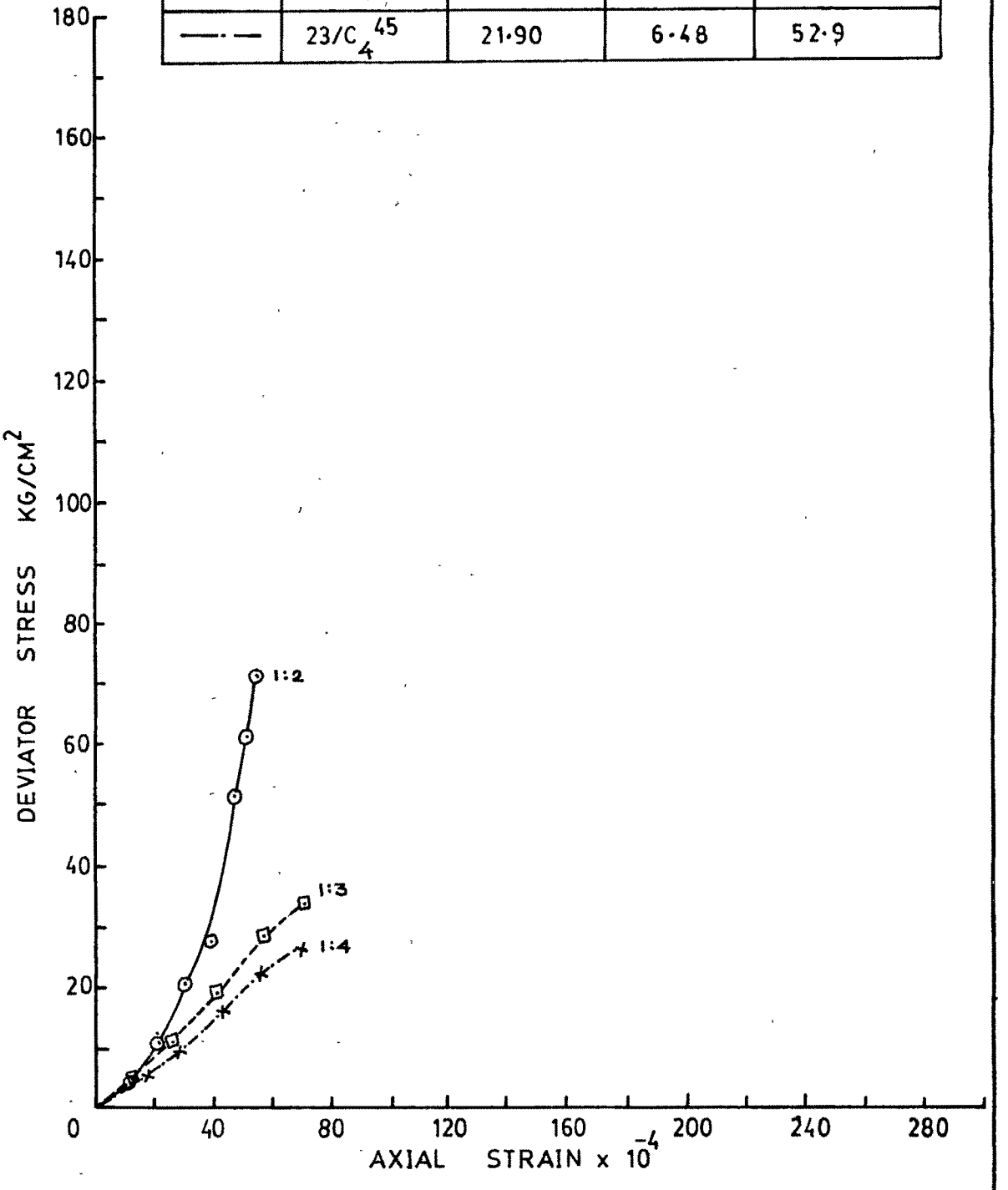

FIG. 6·19 DEVIATOR STRESS AXIAL STRAIN CHARACTERISTIC CURVE

	DESIGNATION	DEVIATOR STRESS AT FAILURE kg/cm^2	STRESS RATIO AT FAILURE σ_1/σ_3	AXIAL STRAIN AT FAILURE 10^{-4}
———	$6/A_6^{45}$	76·68	13·68	45·73
- - - - -	$15/B_6^{45}$	56·64	10·44	23·17
—·—	$24/C_6^{45}$	30·54	6·09	22·48

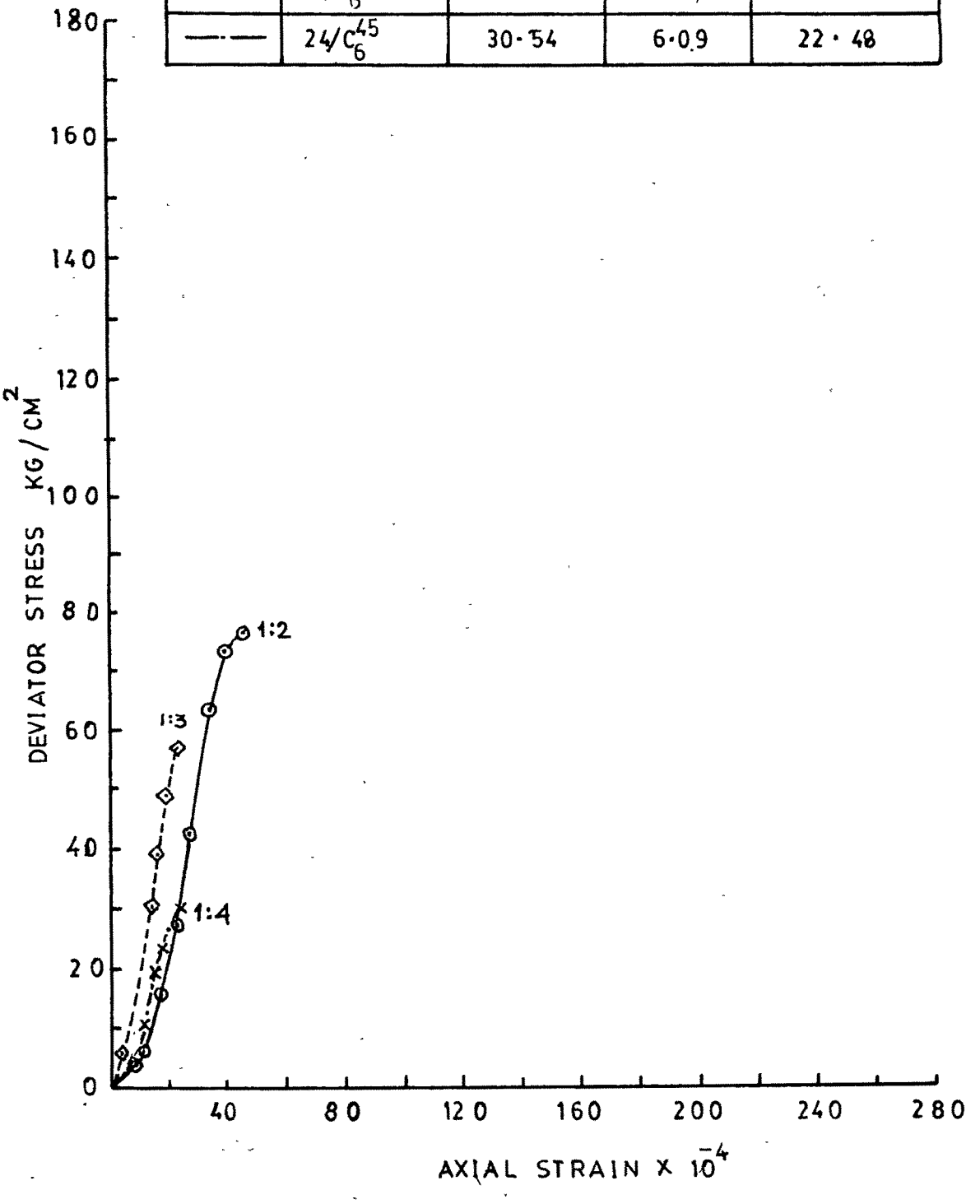

FIG. 6·20 DEVIATOR STRESS AXIAL STRAIN CHARACTERISTIC CURVE

	DESIGNATION	DEVIATOR STRESS AT FAILURE kg/cm^2	STRESS RATIO AT FAILURE σ_1/σ_3	AXIAL STRAIN AT FAILURE 10^{-4}
———	$7/A_2^{30}$	84·84	43·43	170·40
- - - - -	$16/A_2^{30}$	43·50	22·75	121·56
—·—	$25/A_2^{30}$	80·21	41·11	128·74

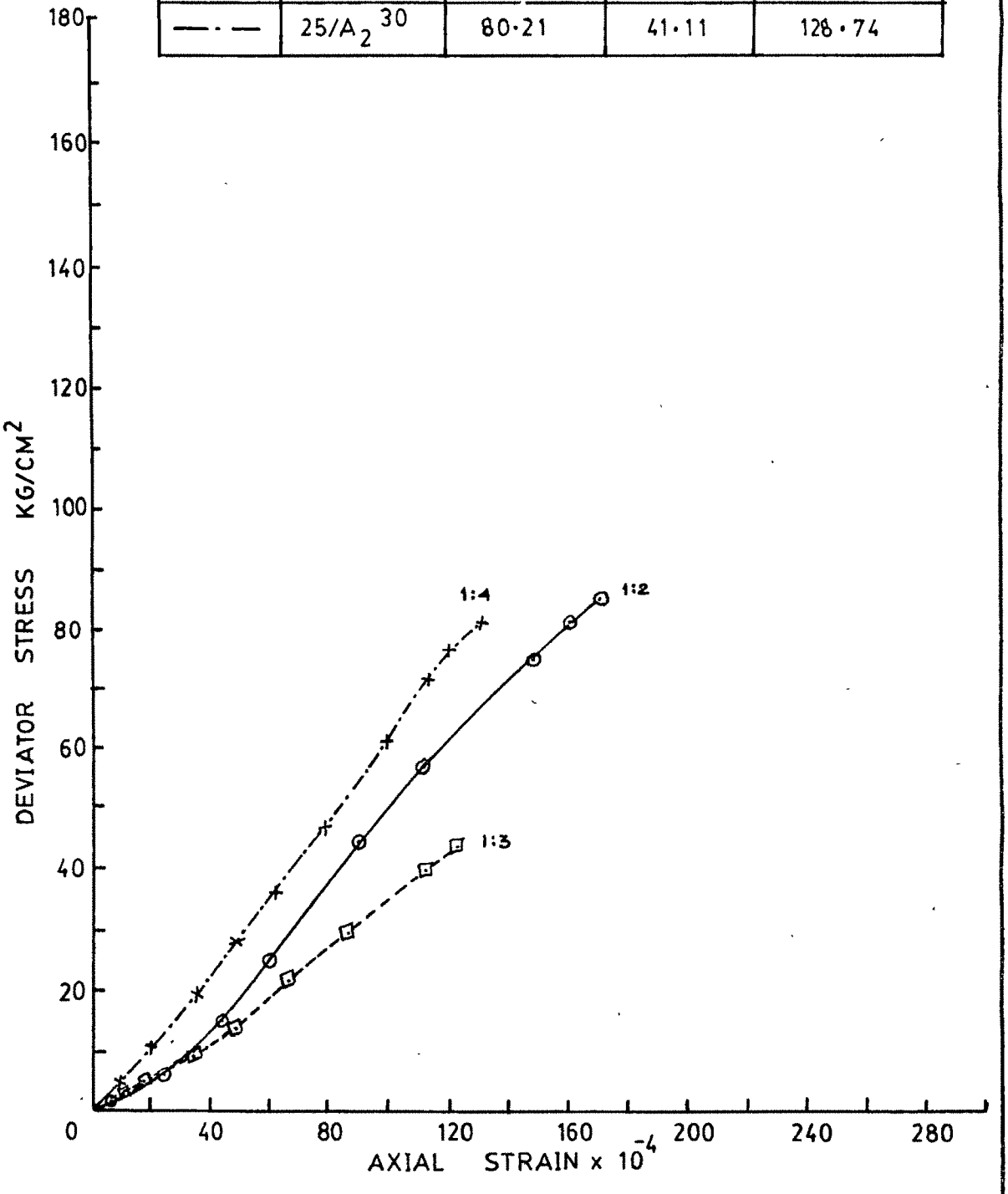

FIG.6-21 DEVIATOR STRESS AXIAL STRAIN CHARACTERISTIC CURVE

	DESIGNANION	DEVIATOR STRESS AT FAILURE kg/cm²	STRESS RATIO AT FAILURE σ_1/σ_3	AXIAL STRAIN AT FAILURE 10^{-4}
———	$8/A_4^{30}$	188·81	48·20	106·10
- - - - -	$17/B_4^{30}$	90·70	23·68	171·00
—·—	$26/C_4^{30}$	83·60	21·90	163·06

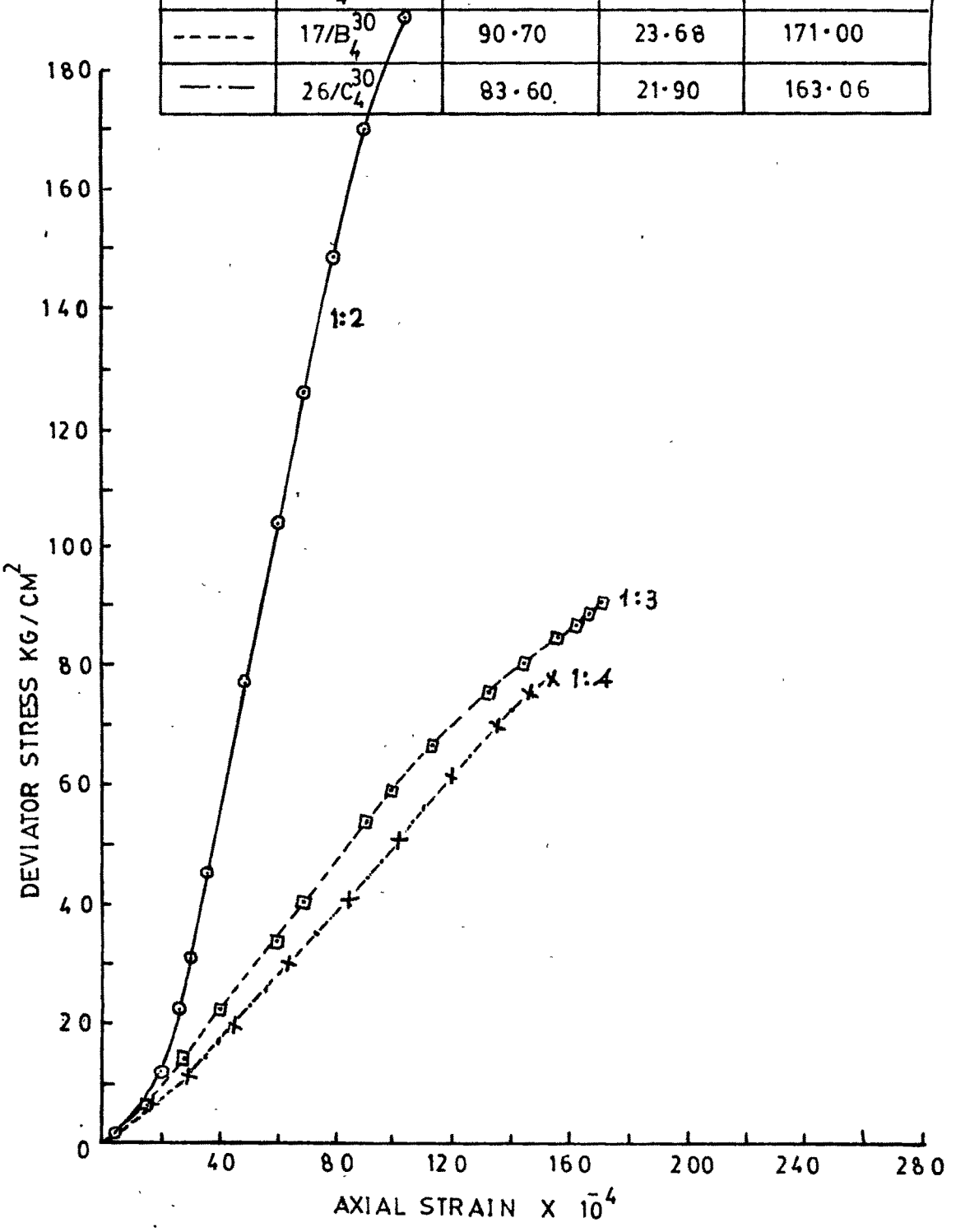

FIG 6-22 DEVIATOR STRESS AXIAL STRAIN CHARACTERISTIC CURVE

	DESIGNATION	DEVIATOR STRESS AT FAILURE kg/cm²	STRESS RATIO AT FAILRE σ_1/σ_3	AXIAL STRAIN AT FAILURE 10^{-4}
———	$9/A_6^{30}$	277·61	141·83	200·00
- - - - -	$18/B_6^{30}$	112·17	19·70	65·4
—·—	$27/C_6^{30}$	29·43	5·91	28·0

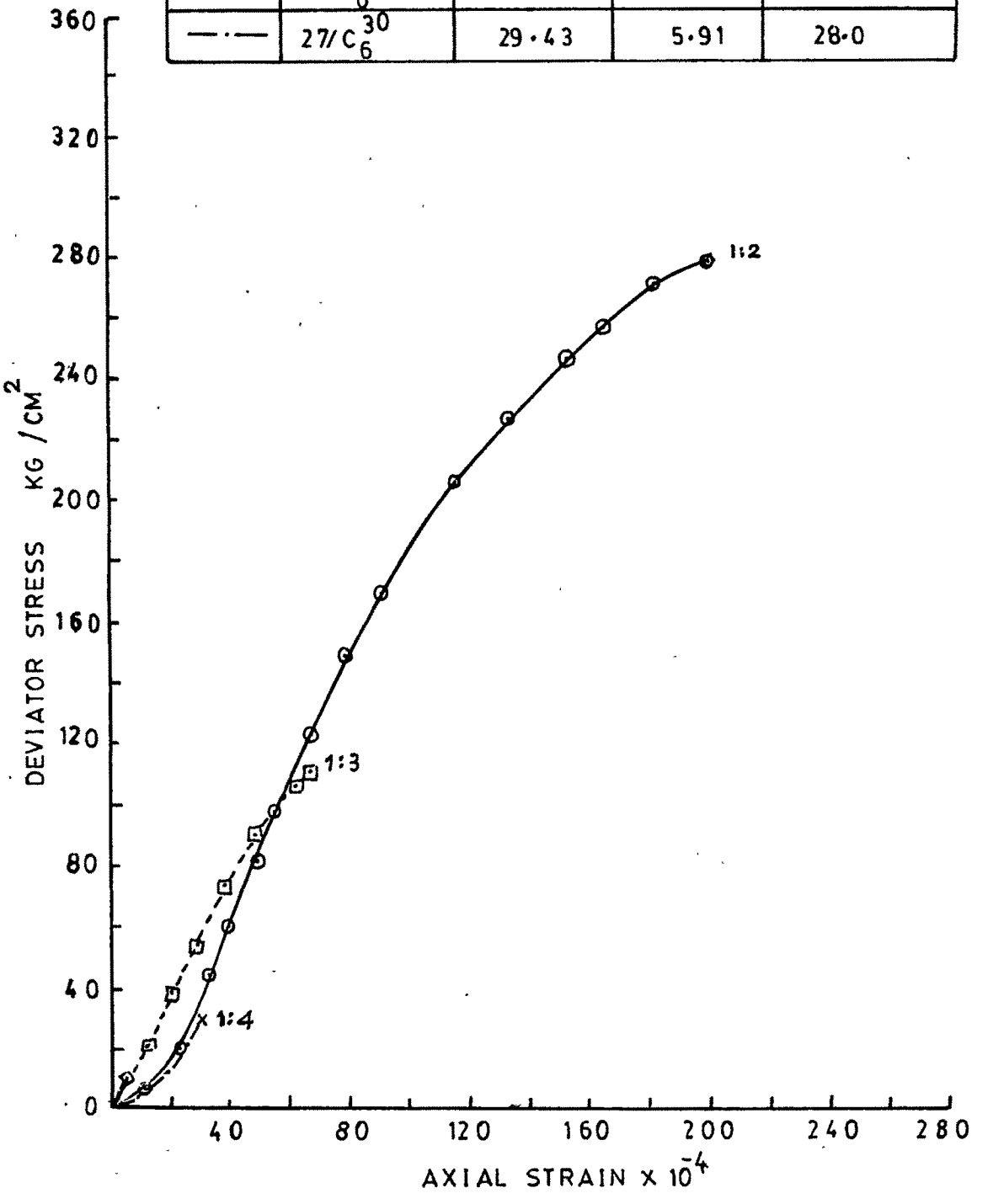

FIG. 6·23 DEVIATOR STRESS AXIAL STRAIN CHARACTERISTIC CURVE

	DESIGNATION	DEVIATOR STRAIN AT FAILURE kg/cm^2	STRESS RATIO AT FAILURE σ_1/σ_3	AXIAL STRAIN AT FAILURE 10^{-4}
———	$28/X_2^{54.8}$	17.08	9.54	23.93
- - - - -	$32/Y_2^{54.8}$	4.60	3.30	14.96
—·—	$36/Z_2^{54.8}$	3.17	2.59	20.13

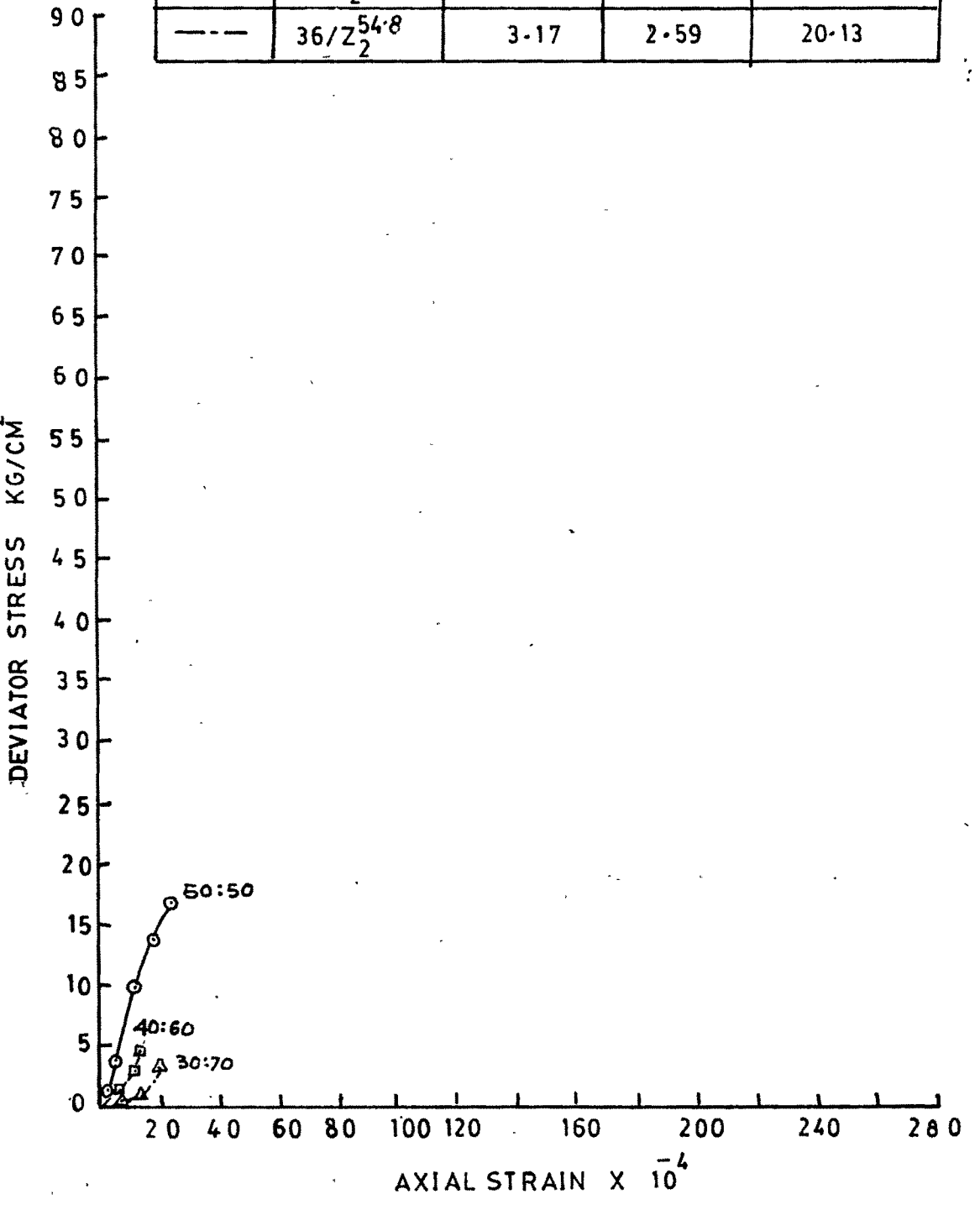

FIG. 6·24 DEVIATOR STRESS AXIAL STRAIN CHARACTERISTIC CURVE

	DESIGNATION	DEVIATOR STRESS AT FAILURE kg/cm^2	STRESS RATIO AT FAILURE σ_1/σ_3	AXIAL STRAIN AT FAILURE 10^{-4}
———	$29/X_4^{54\cdot8}$	21·84	6·46	61·73
- - - - -	$33/Y_4^{54\cdot8}$	15·18	4·80	56·00
— - —	$37/Z_4^{54\cdot8}$	3·80	1·95	12·09

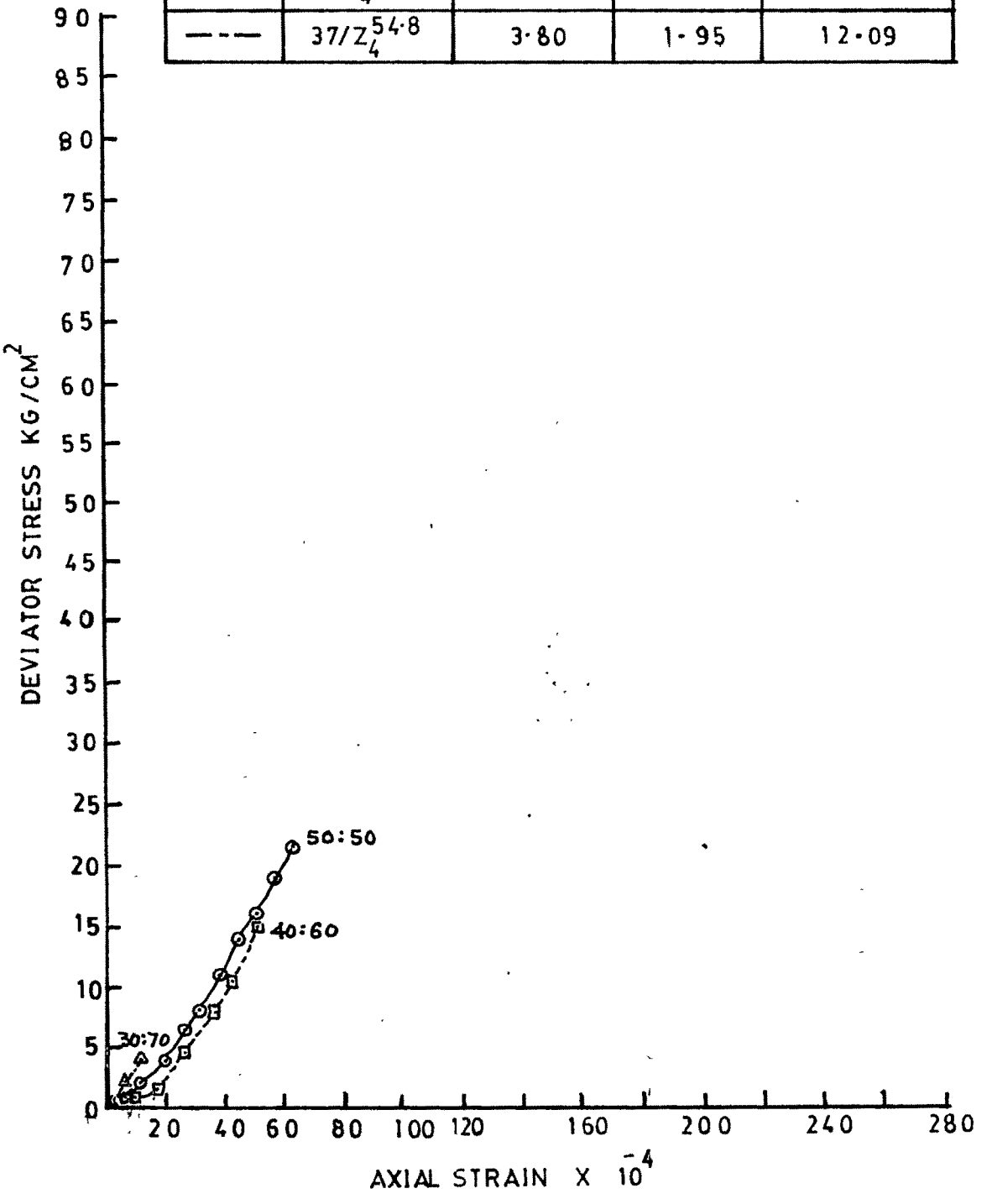

FIG. 6-25 DEVIATOR STRESS AXIAL STRAIN CHARACTERISTIC CURVE

	DESIGNATION	DEVIATOR STRESS AT FAILURE kg/cm^2	STRESS RATIO AT FAILURE σ_1/σ_3	AXIAL STRAIN AT FAILURE 10^{-4}
———	$30/X_6^{54\cdot8}$	25·07	5·18	64·07
- - - - -	$34/Y_6^{54\cdot8}$	11·27	2·88	50·00
—·—	$38/Z_6^{54\cdot8}$	16·33	3·72	54·73

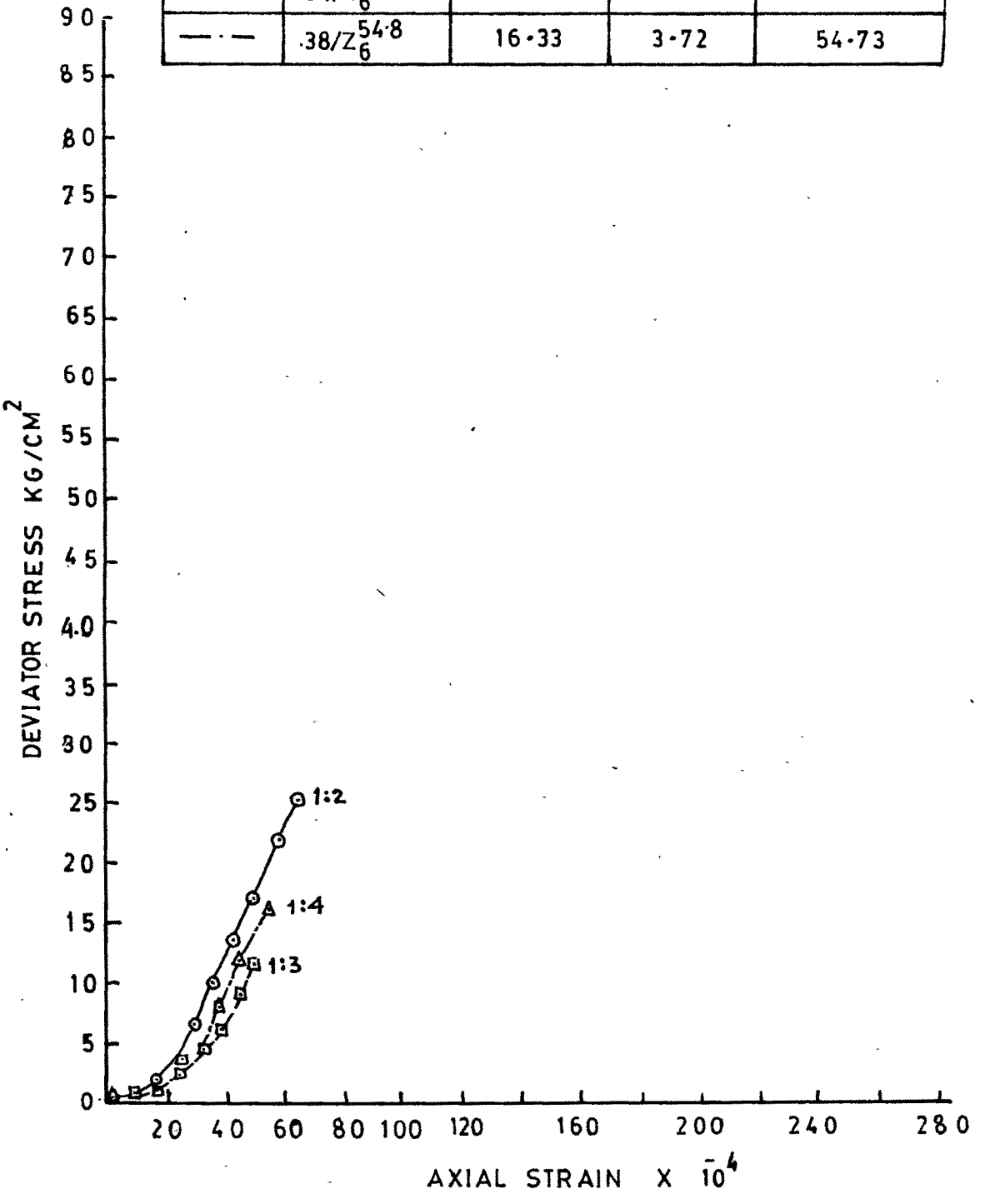

FIG. 6·26 DEVIATOR STRESS AXIAL STRAIN CHARACTERISTIC CURVE

	DESIGNATION	DEVIATOR STRESS AT FAILURE kg/cm^2	STRESS RATIO AT FAILURE σ_1/σ_3	AXIAL STRAIN AT FAILURE 10^{-4}
———	$31/X_8^{54.8}$	43.01	6.38	96.71
- - - - -	$35/Y_8^{54.8}$	38.46	5.80	80.13
—·—	$39/Z_8^{54.8}$	18.86	3.30	36.42

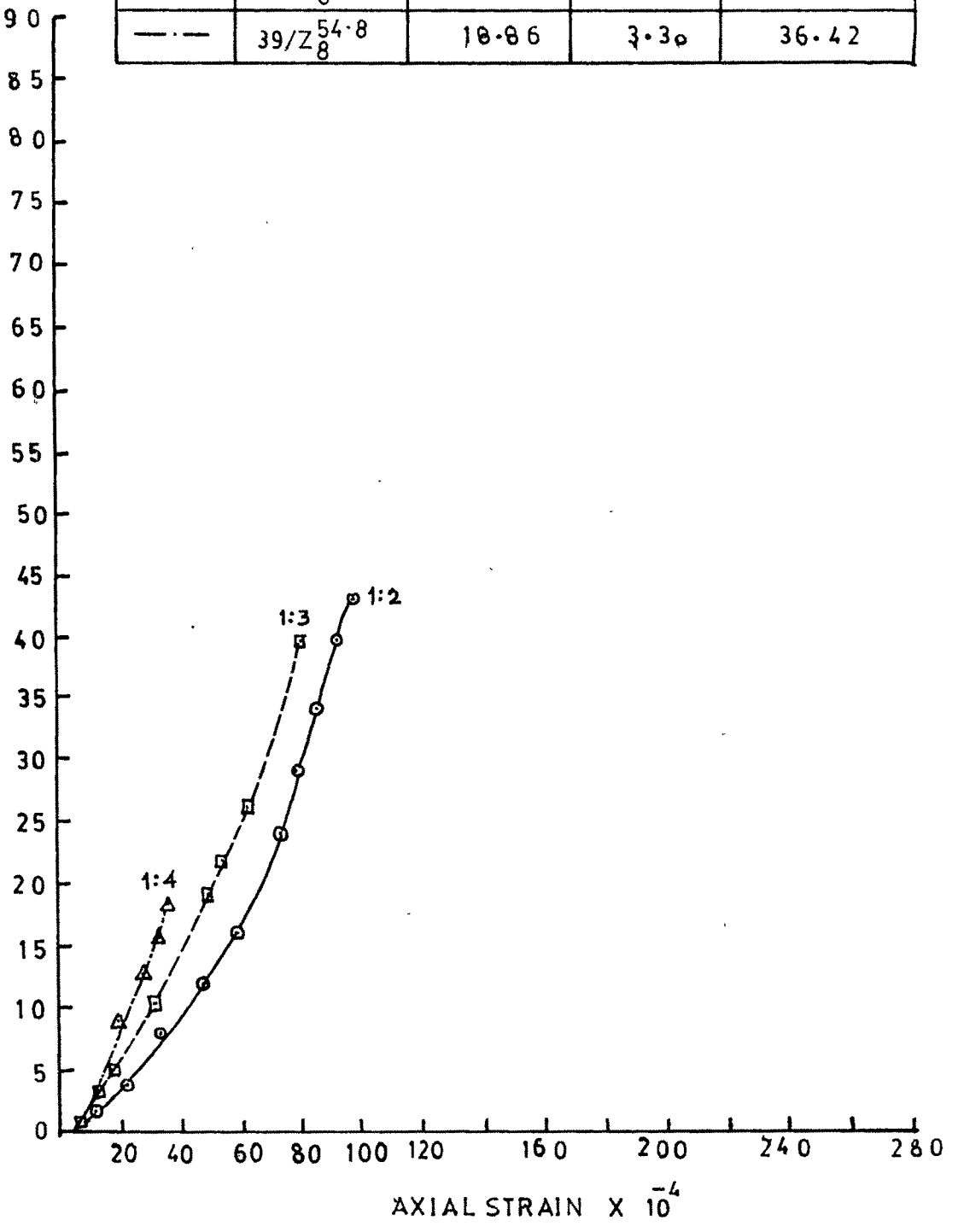

FIG.6.27 DEVIATOR STRESS AXIAL STRAIN CHARACTERISTIC CURVE

	DESIGNATION	DEVIATOR STRESS AT FAILURE kg/m^2	STRESS RATIO AT FAILURE σ_1/σ_3	AXIAL STRAIN AT FAILURE 10^{-4}
———	$40/XX_2^{54\cdot8}$	9·85	5·93	18·66
- - - - -	$44/YY_2^{54\cdot8}$	4·85	3·925	32·06
—·—	$48/ZZ_2^{54\cdot8}$	8·47	5·235	14·81

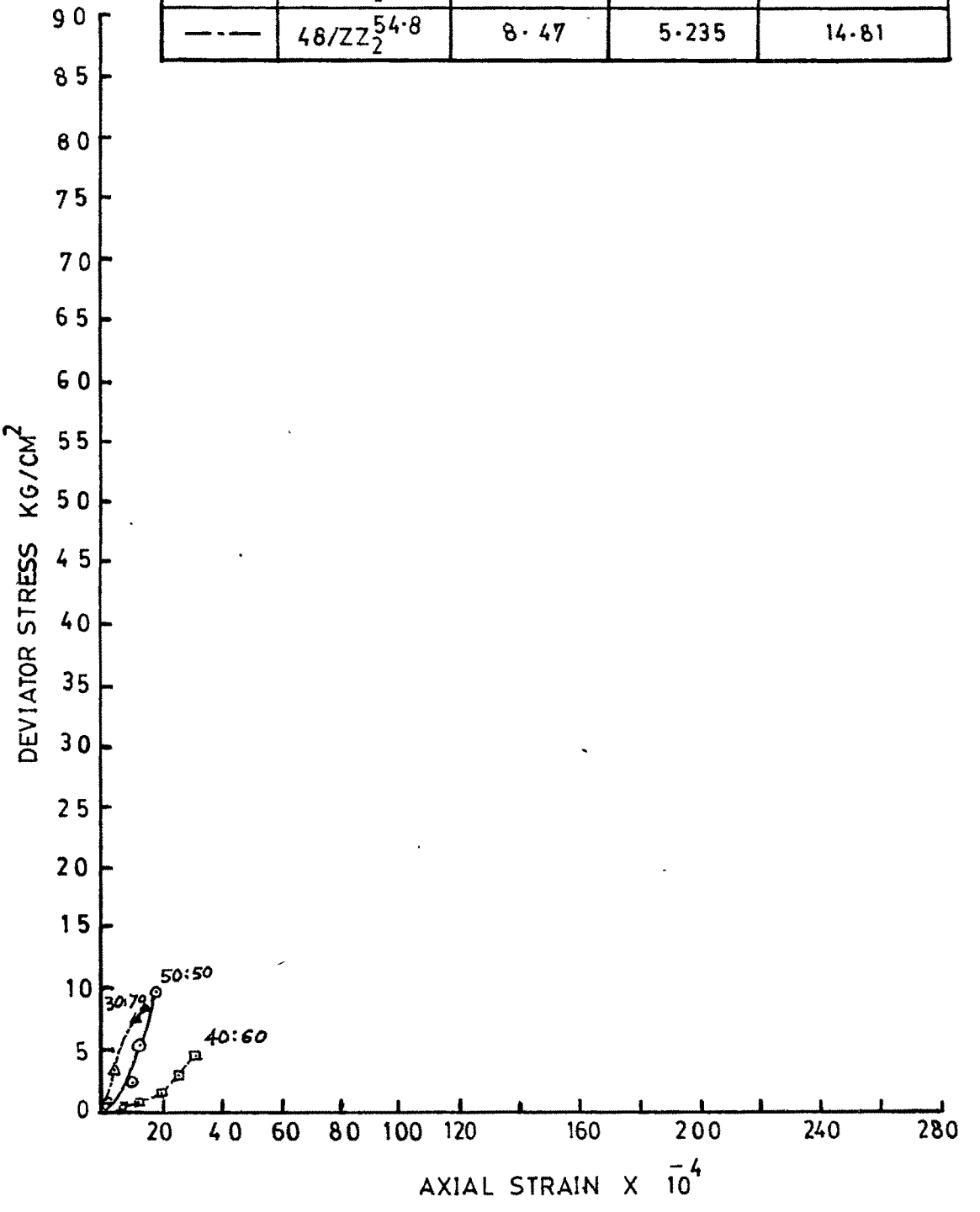

FIG.6·28 DEVIATOR STRESS AXIAL STRAIN CHARACTERISTIC CURVE

	DESIGNATION	DEVIATOR STRESS AT FAILURE kg/cm^2	STRESS RATIO AT FAILURE σ_1/σ_3	AXIAL STRAIN AT FAILURE 10^{-4}
———	$41/XX_4^{54\cdot8}$	13·43	4·36	45·59
- - - -	$45/YY_4^{54\cdot8}$	10·67	3·67	18·66
—·—	$49/ZZ_4^{54\cdot8}$	5·74	2·44	23·48

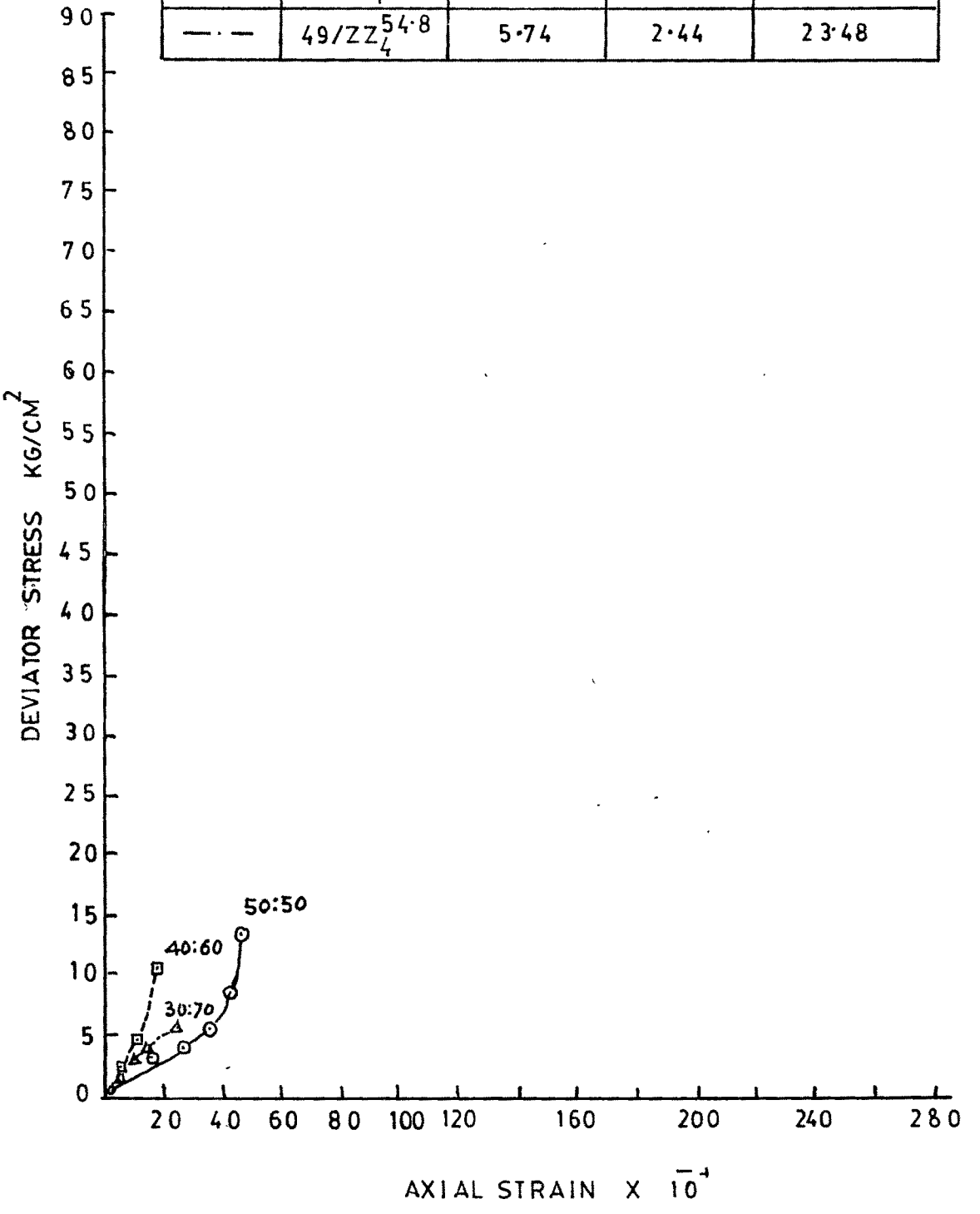

FIG.6·29 DEVIATOR STRESS AXIAL STRAIN CHARACTERISTIC CURVE

	DESIGNATION	DEVIATOR STRAIN AT FAILURE kg/cm^2	STRESS RATIO AT FAILURE σ_1/σ_3	AXIAL STAIN AT FAILURE 10^{-4}
———	$42/XX_6^{54\cdot8}$	18·23	4·03	66·43
- - - - -	$46/YY_6^{54\cdot8}$	12·31	3·05	20·98
—·—	$50/ZZ_6^{54\cdot8}$	11·49	2·92	35·07

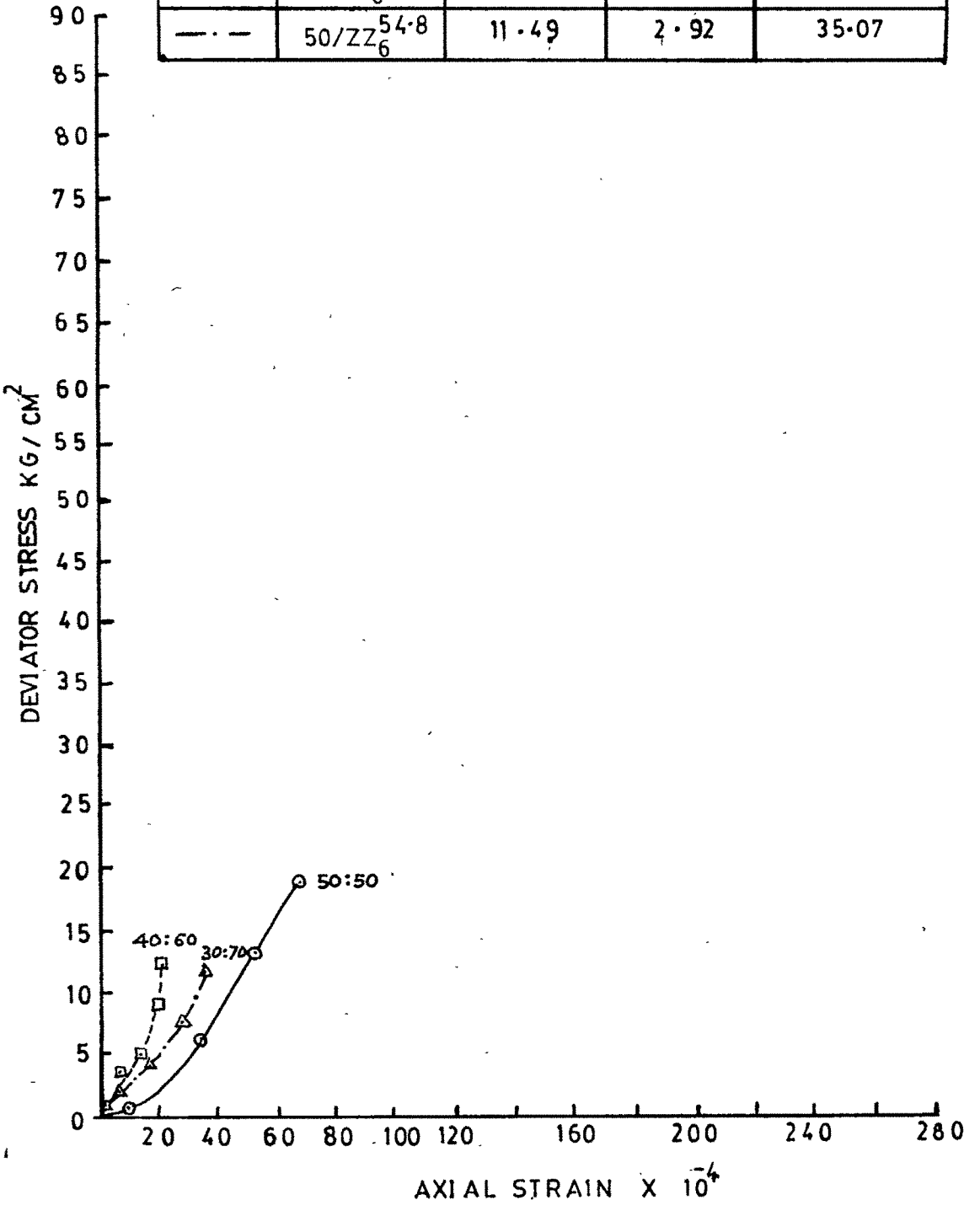

FIG.6-30 DEVIATOR STRESS AXIAL STRAIN CHARACTERSTIC CURVE

	DESIGNATION	DEVIATOR STRAIN AT FAILURE kg/cm^2	STRESS RATIO AT FAILURE σ_1/σ_3	AXIAL STRAIN AT FAILURE 10^{-4}
——	$43/XX_8^{54\cdot8}$	18·05	3·26	25·64
- - - - -	$47/YY_8^{54\cdot8}$	14·77	2·85	28·66
—·—	$51/ZZ_8^{54\cdot8}$	43·50	6·44	32·08

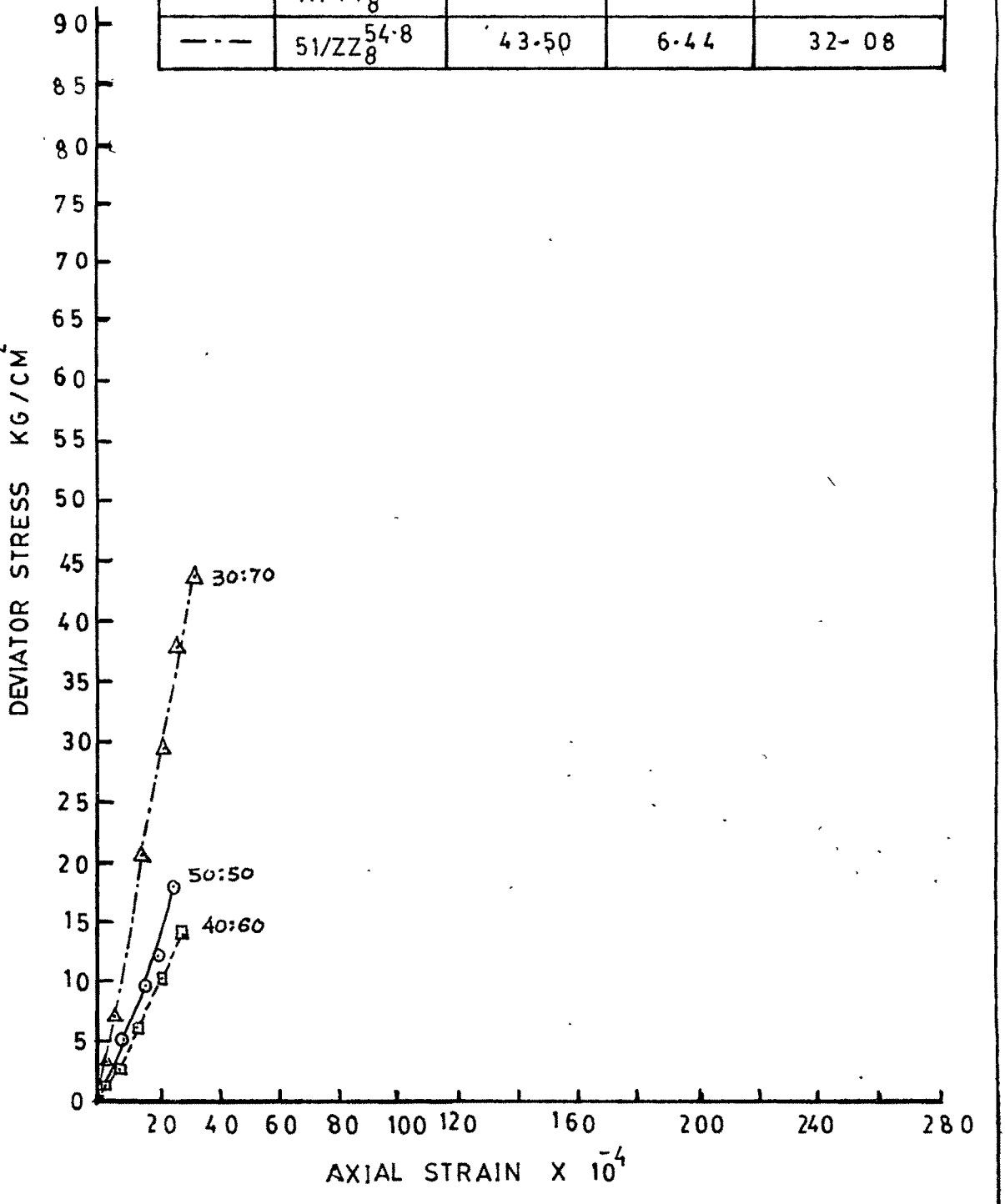

FIG. 6·31 DEVIATOR STRESS AXIAL STRAIN CHARACTERISTIC CURVE

30:70 at 54.8° joint orientations and tested under cell pressures 2 kg/cm^2, 4 kg/cm^2 and 6 kg/cm^2 and 8 kg/cm^2 for N_x size specimens and figure 6.28 to 6.31 represents similar gouge materials, joint orientation and cell pressures but for A_x size specimens. In most of the cases the failure was instantaneous and associated with characteristic thud noise. The nature of most of the stress-strain curve is similar having concave downward nature in early stage and a slight concave upward nature in peak region. For all proportions of cement:bentonite gouge materials the concave downward portion in early stage is very predominant while concave upward portion is very less or absent in peak region. The plots also show that in gouge material having proportions 40:60 and 30:70 cement:bentonite the samples fail in concave downward region only. The similar characteristic are observed for both the N_x and A_x specimens. In almost all cases the stronger material exhibits lower strain at same stress level in comparision with weak gouge material. From the observations the influence of mechanical properties of the gouge material on the shearing behaviour of the specimens is indicative since the effect of confining pressure on cement sand is much less predominant compared to that on cement . bentonite gouge material.

6.4.3 Category - III

Figures 6.32 to 6.43 show graphically stress strain characteristic curves along with tables of principal values of stress and strain at failure. Figures 6.32 to 6.43 show the stress-strain curves for specimens filled with same

	DESIGNATION	DEVIATOR STRESS AT FAILURE kg/cm^2	STRESS RATIO AT FAILURE $\frac{\sigma_1}{\sigma_3}$	AXIAL STRAIN AT FAILURE 10^{-4}
———	$28/X_2^{54\cdot8}$	17·08	9·54	23/93
- - - -	$40/XX_2^{54\cdot8}$	9·85	5·93	18·66

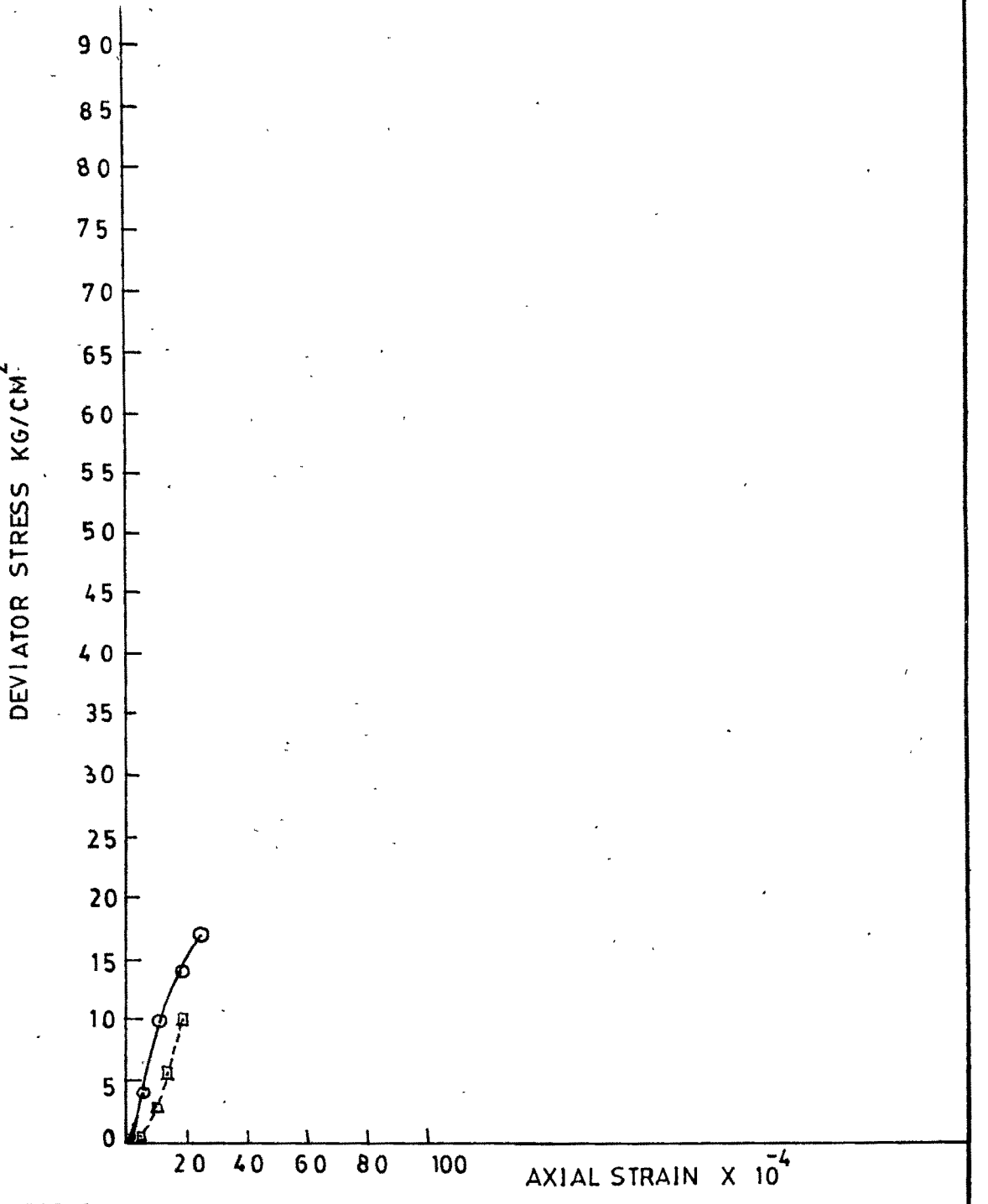

FIG.6-32 DEVIATOR STRESS AXIAL STRAIN CHARACTERISTIC CURVE

	DESIGNATION	DEVIATOR STRESS AT FAILURE kg/cm²	STRESS RATIO AT FAILURE σ_1/σ_3	AXIAL STRAIN AT FAILURE 10^{-4}
———	$29/X_4^{54.8}$	21·84	6·46	61·73
- - - -	$41/XX_4^{54.8}$	13·43	4·36	45·59

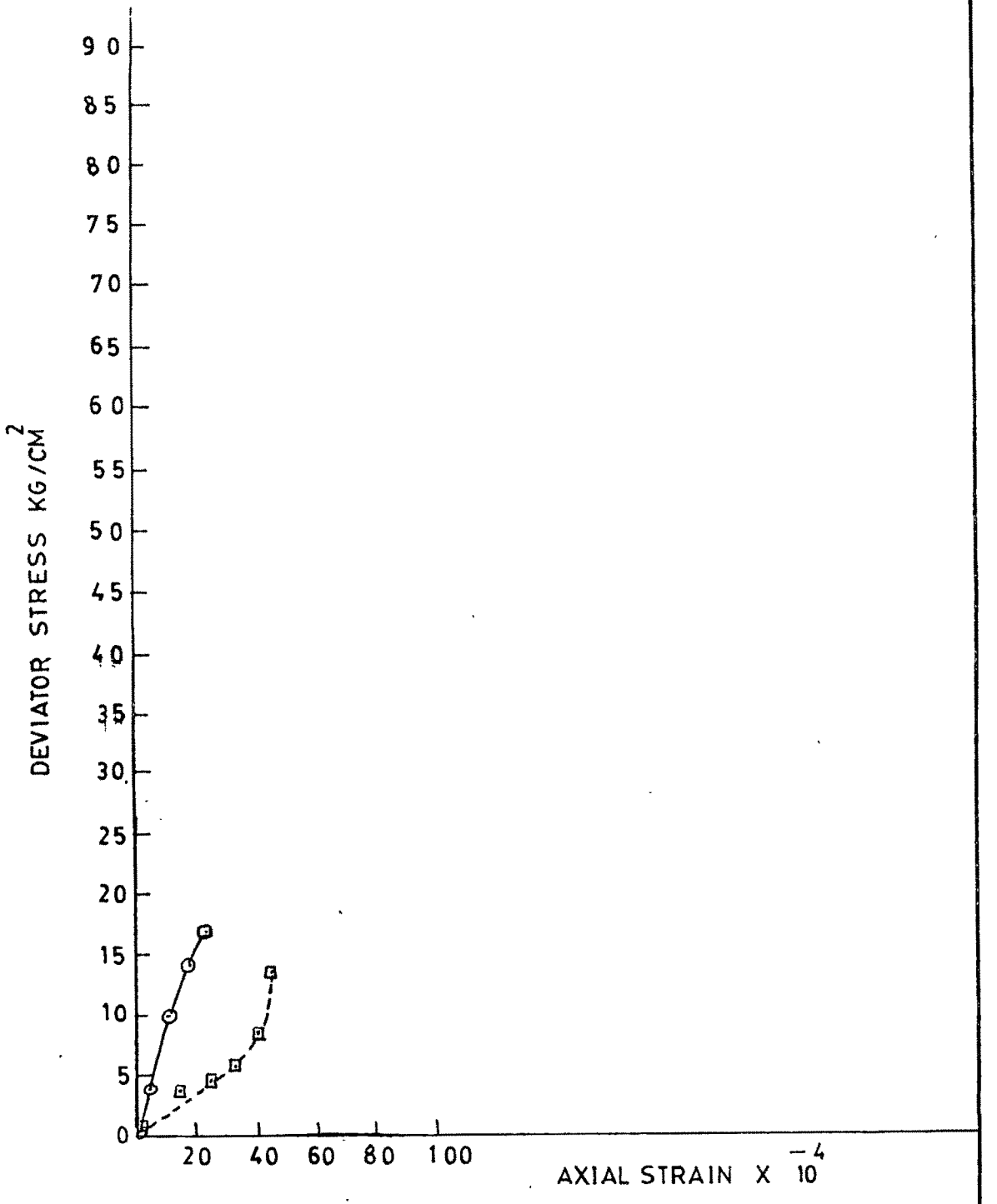

FIG. 6·33 DEVIATOR STRESS AXIAL STRAIN CHARACTERISTIC CURVE

	DESIGNATION	DEVIATOR STRESS AT FAILURE kg/cm^2	STRESS RATIO AT FAILURE $\frac{\sigma_1}{\sigma_3}$	AXIAL STRAIN AT FAILURE 10^{-4}
———	$30/X_6^{54.8}$	25.07	5.18	64.07
- - - -	$42/XX_6^{54.8}$	18.23	4.03	66.43

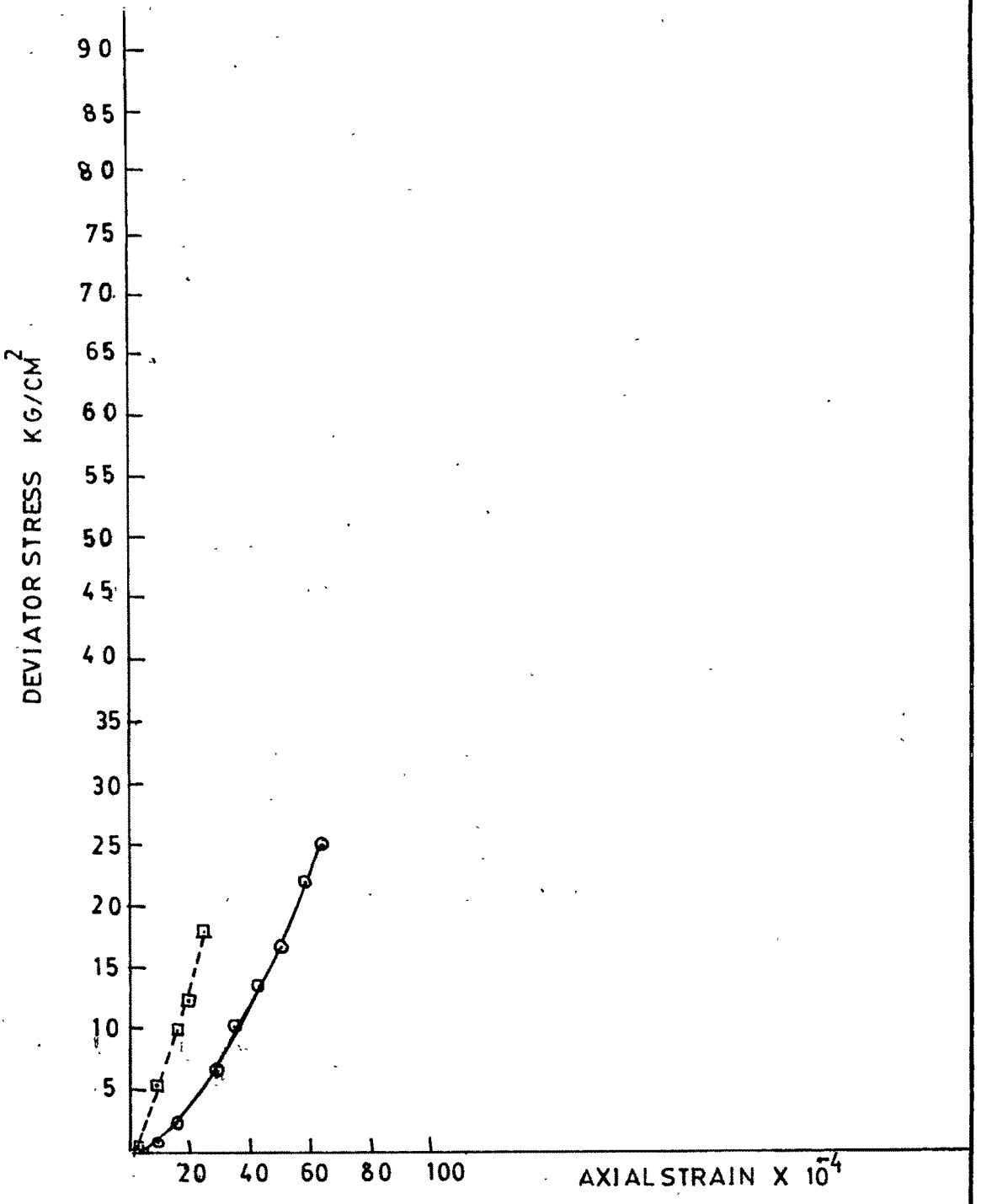

FIG. 6.34 DEVIATOR STRESS AXIAL STRAIN CHARACTERISTIC CURVE

	DESIGNATION	DEVIATOR STRESS AT FAILURE kg/cm^2	STRESS RATIO AT FAILURE σ_1/σ_3	AXIAL STRAIN AT FAILURE 10^{-4}
———	$31/X_8^{54\cdot8}$	43·01	6·38	96·71
- - - -	$43/XX_8^{54\cdot8}$	18·05	3·26	25·64

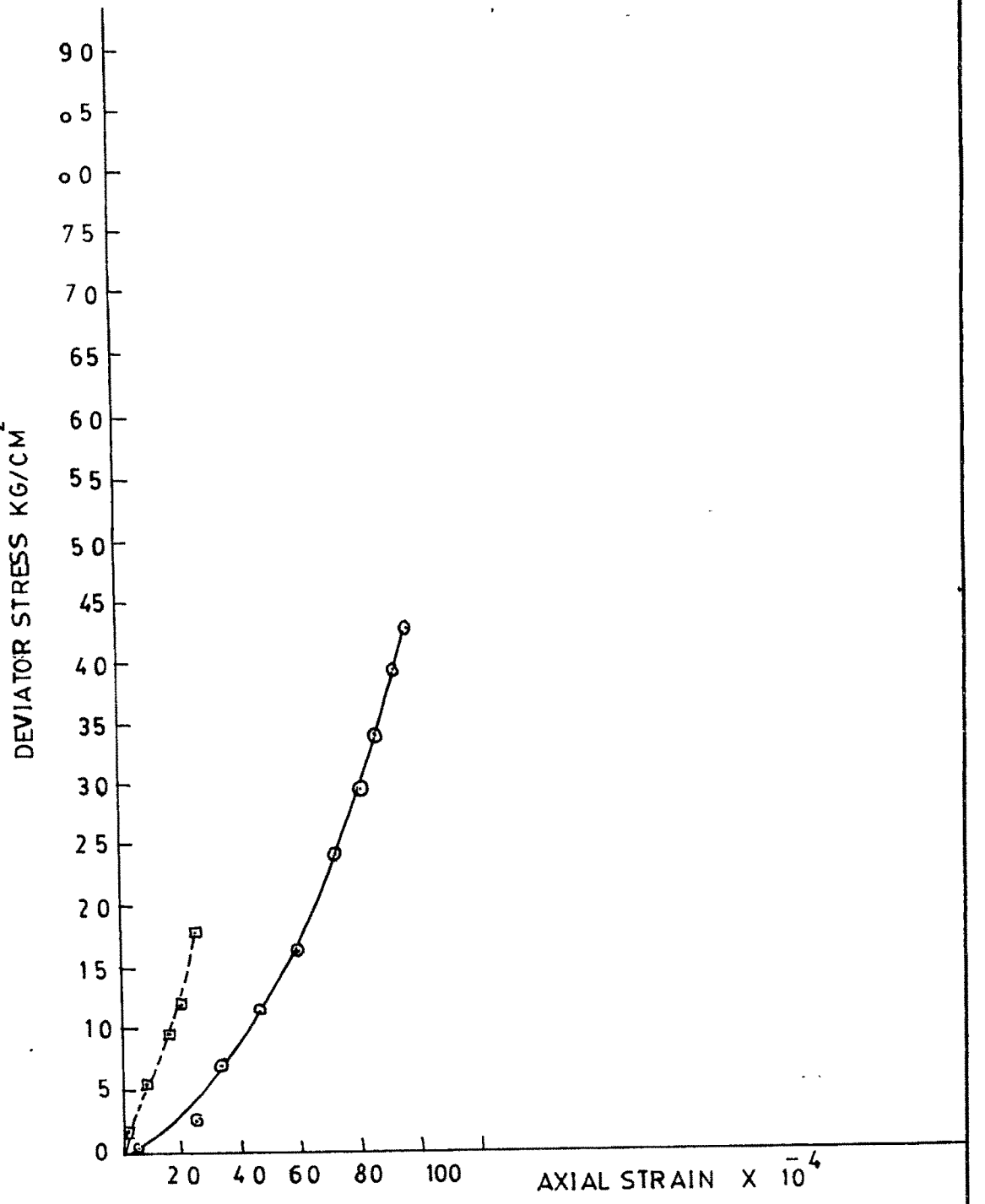

FIG. 6·35 DEVIATOR STRESS AXIAL STRAIN CHARACTERISTIC CURVE

	DESIGNATION	DEVIATOR STRESS AT FAILURE Kg/cm^2	STRESS RATIO AT FAILURE σ_1/σ_3	AXIAL STRAIN AT FAILURE 10^{-4}
———	$32/Y_2^{54\cdot8}$	4·60	3·30	14·96
– – – –	$44/YY_2^{54\cdot8}$	4·85	3·925	32·06

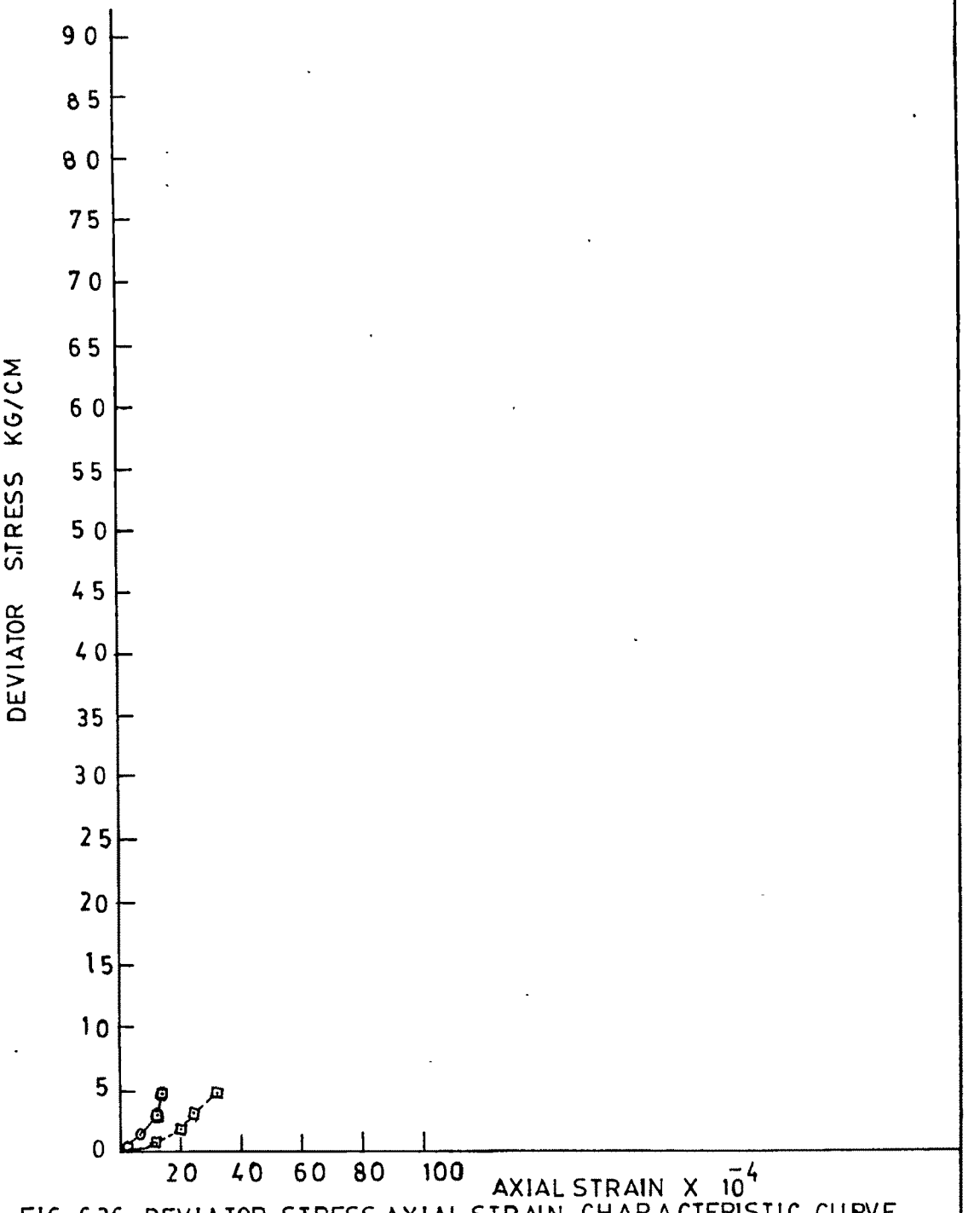

FIG. 6-36 DEVIATOR STRESS AXIAL STRAIN CHARACTERISTIC CURVE

	DESIGNATION	DEVIATOR STRESS AT FAILURE kg/cm²	STRESS RATIO AT FAILURE σ_1/σ_3	AXIAL STRAIN AT FAILURE 10^{-4}
———	$33/Y_4^{54\cdot8}$	15·18	4·80	56·00
- - - -	$45/YY_4^{54\cdot8}$	10·67	3·67	18·66

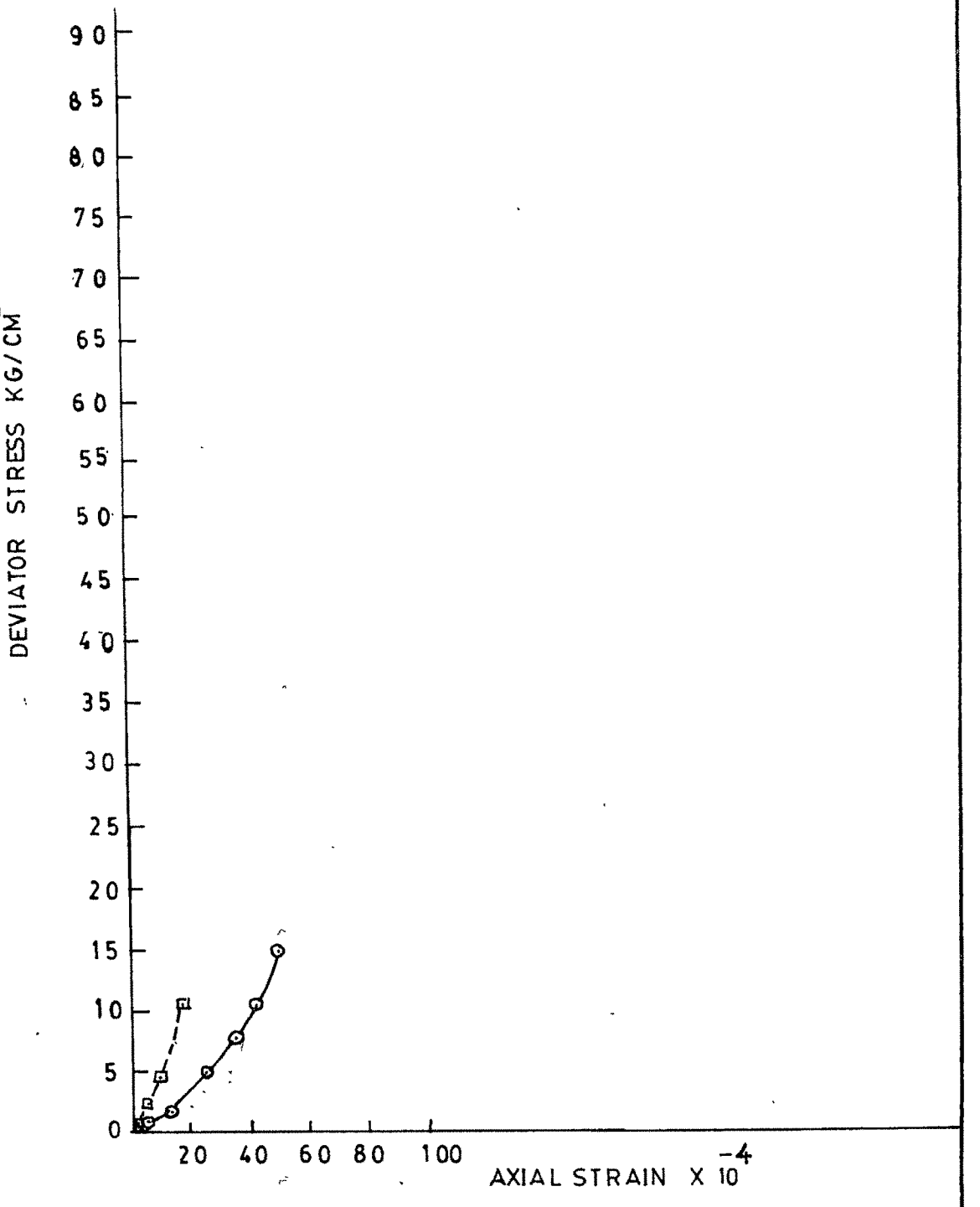

FIG. 6·37 DEVIATOR STRESS AXIAL STRAIN CHARACTERISTIC CURVE

	DESIGNATION	DEVIATOR STRESS AT FAILURE kg/cm^2	STRESS RATIO AT FAILURE σ_1/σ_3	AXIAL STRAIN AT FAILURE 10^{-4}
———	$34/Y_6^{54\cdot8}$	11·27	2·88	50·00
– – – –	$46/YY_6^{54\cdot8}$	12·31	3·05	20·98

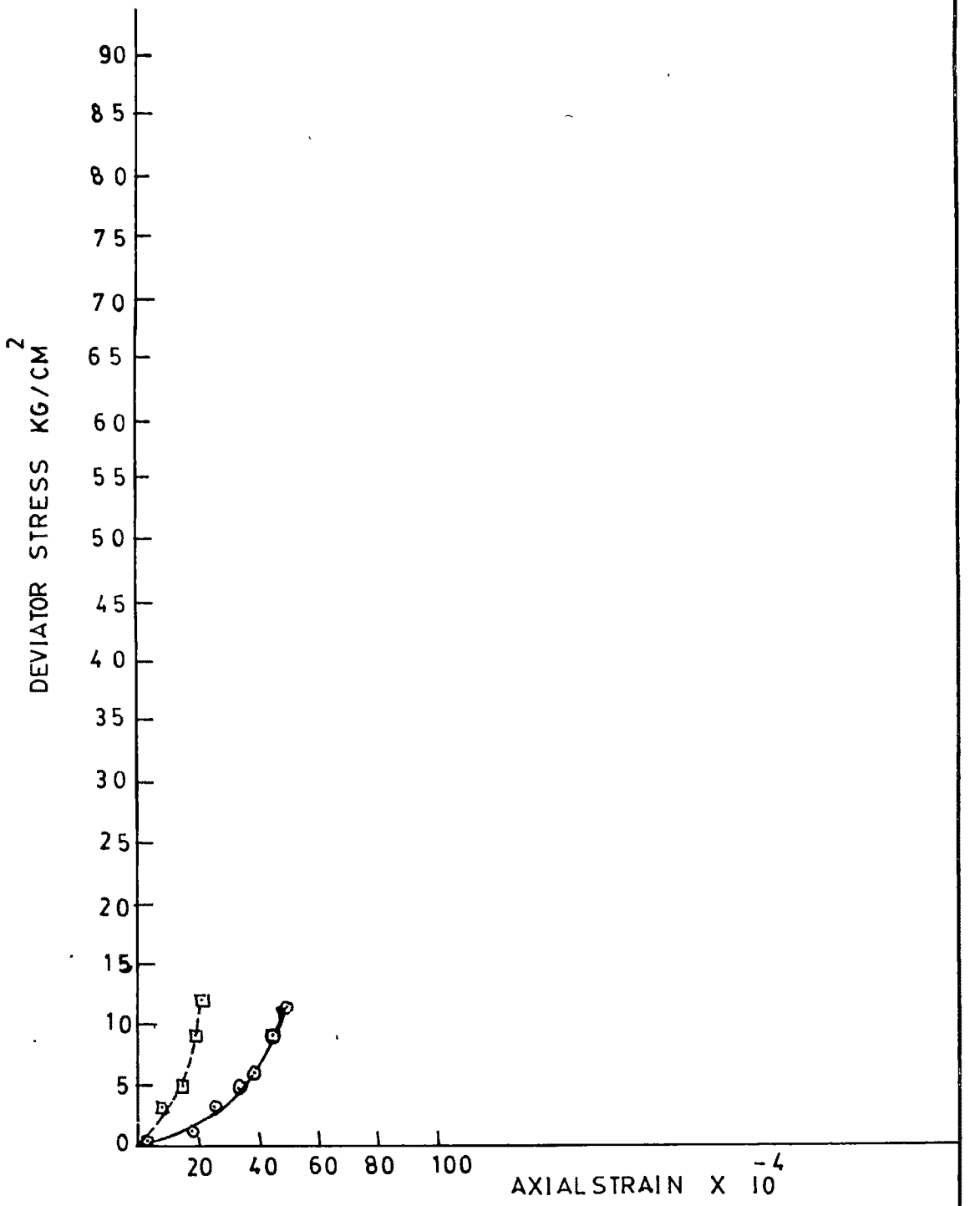

FIG.6·38 DEVIATOR STRESS AXIALSTRAIN CHARACTERISTIC CURVE

	DESIGNATION	DEVIATOR STRESS AT FAILURE kg/cm^2	STRESS RATIO AT FAILURE σ_1/σ_3	AXIAL STRAIN AT FAILURE 10^{-4}
———	$35/Y_8^{54\cdot8}$	38·46	5·80	80·13
– – –	$47/YY_8^{54\cdot8}$	14·77	2·85	28·66

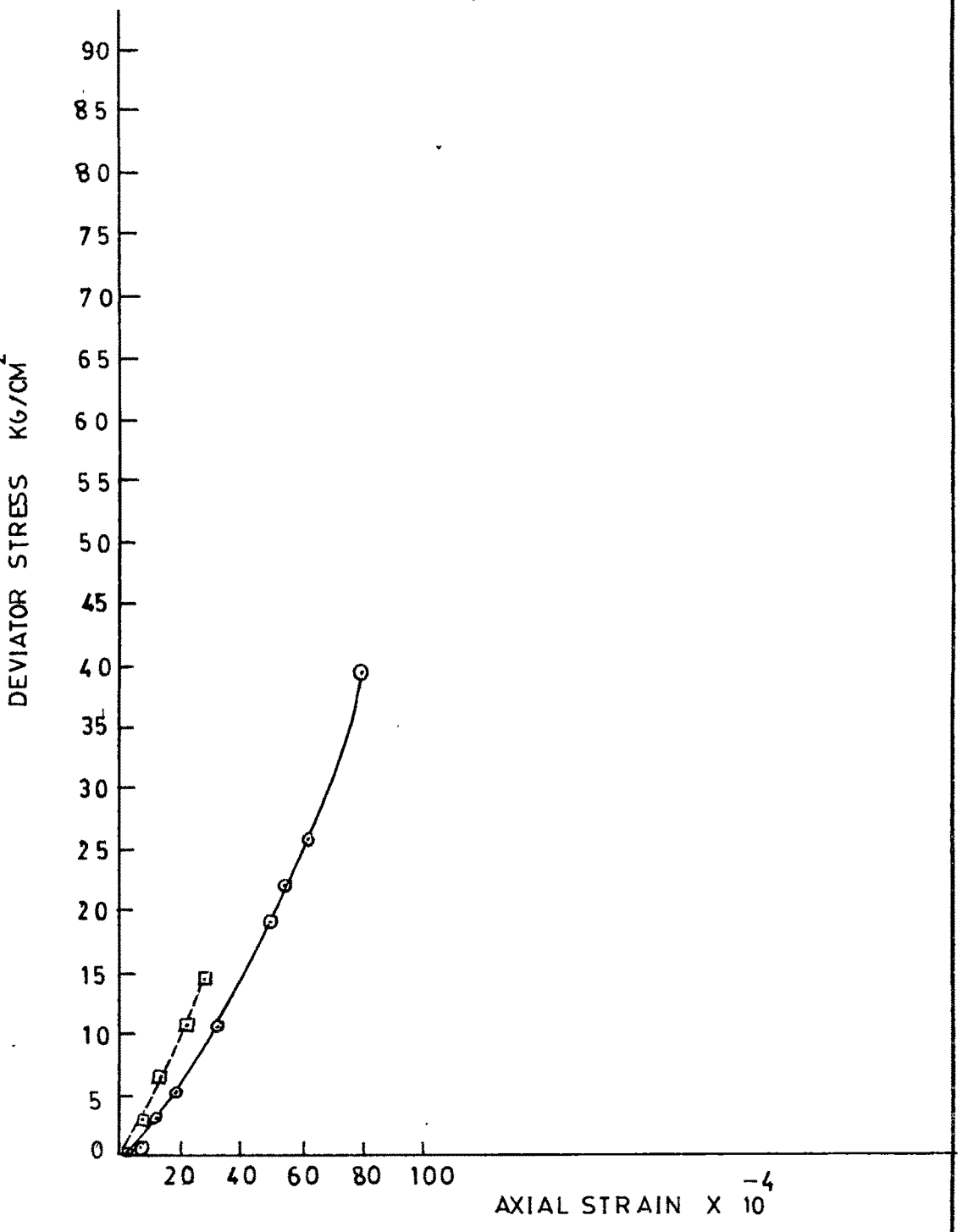

FIG. 6·39 DEVIATOR STRESS AXIAL STRAIN CHARACTERISTIC CURVE

	DESIGNATION	DEVIATOR STRESS AT FAILURE kg/cm^2	STRESS RATIO AT FAILURE σ_1/σ_3	AXIAL STRAIN AT FAILURE 10^{-4}
———	$36/Z_2^{54\cdot8}$	3·17	2·59	20·13
- - - -	$48/ZZ_2^{54\cdot8}$	8·47	5·235	14·81

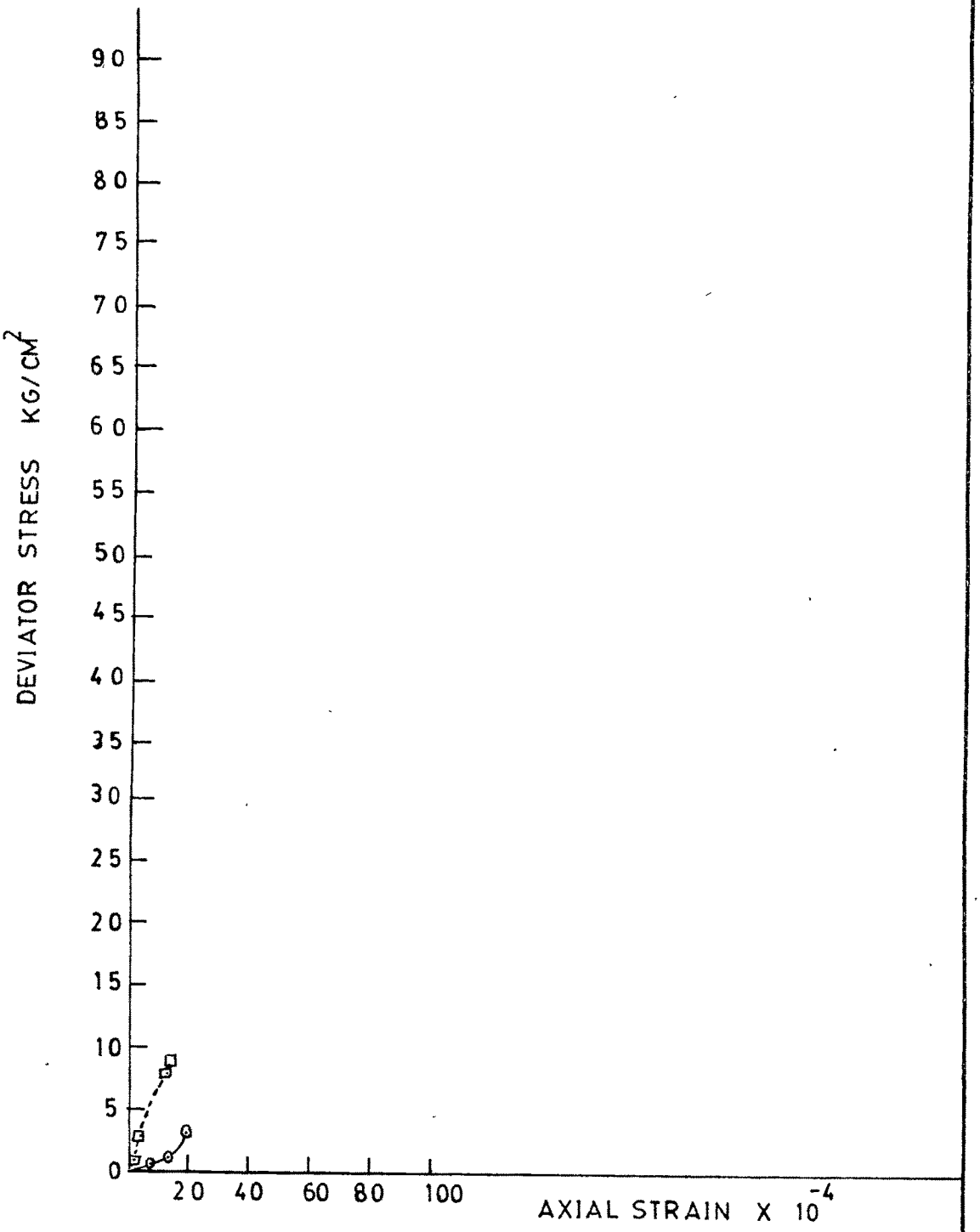

FIG. 6·40 DEVIATOR STRESS AXIAL STRAIN CHARACTERISTIC CURVE

		DEVIATOR STRESS AT FAILURE kg/cm^2	STRESS RATIO AT FAILURE σ_1/σ_3	AXIAL STRAIN AT FAILURE 10^{-4}
———	$37/Z_4^{54.8}$	3·80	1·95	12·09
- - - -	$49/ZZ_4^{54.8}$	5·74	2·44	23·48

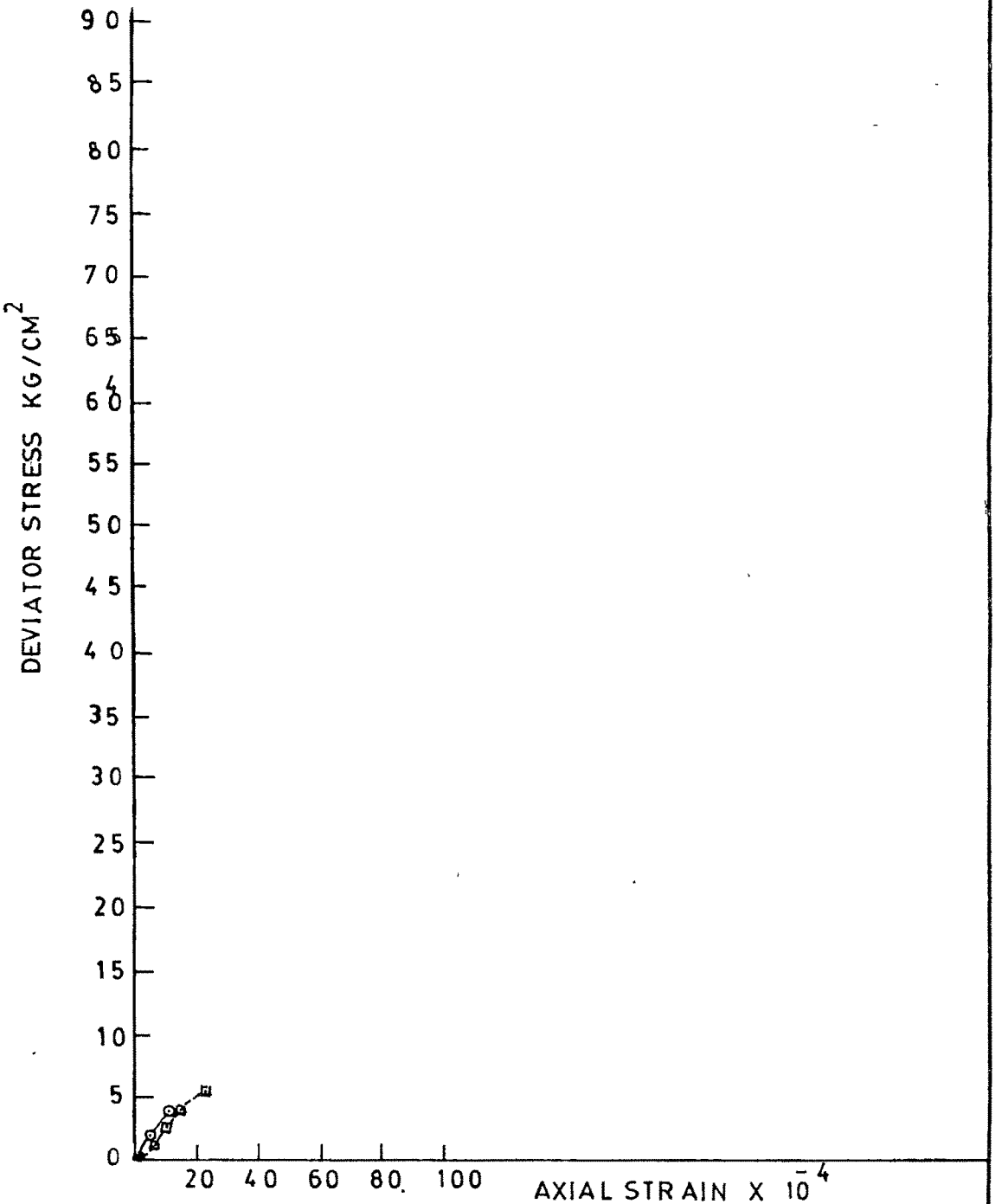

FIG. 6·41 DEVIATOR STRESS AXIAL STRESS CHARACTERISTIC CURVE

	DESIGNATION	DEVIATOR STRESS AT FAILURE kg/cm²	STRESS RATIO AT FAILURE σ_3/σ_1	AXIAL STRAIN AT FAILURE 10^{-4}
———	$38/Z_6^{54\cdot8}$	16·33	3·72	54·73
– – –	$50/ZZ_6^{54\cdot8}$	11·49	2·92	35·07

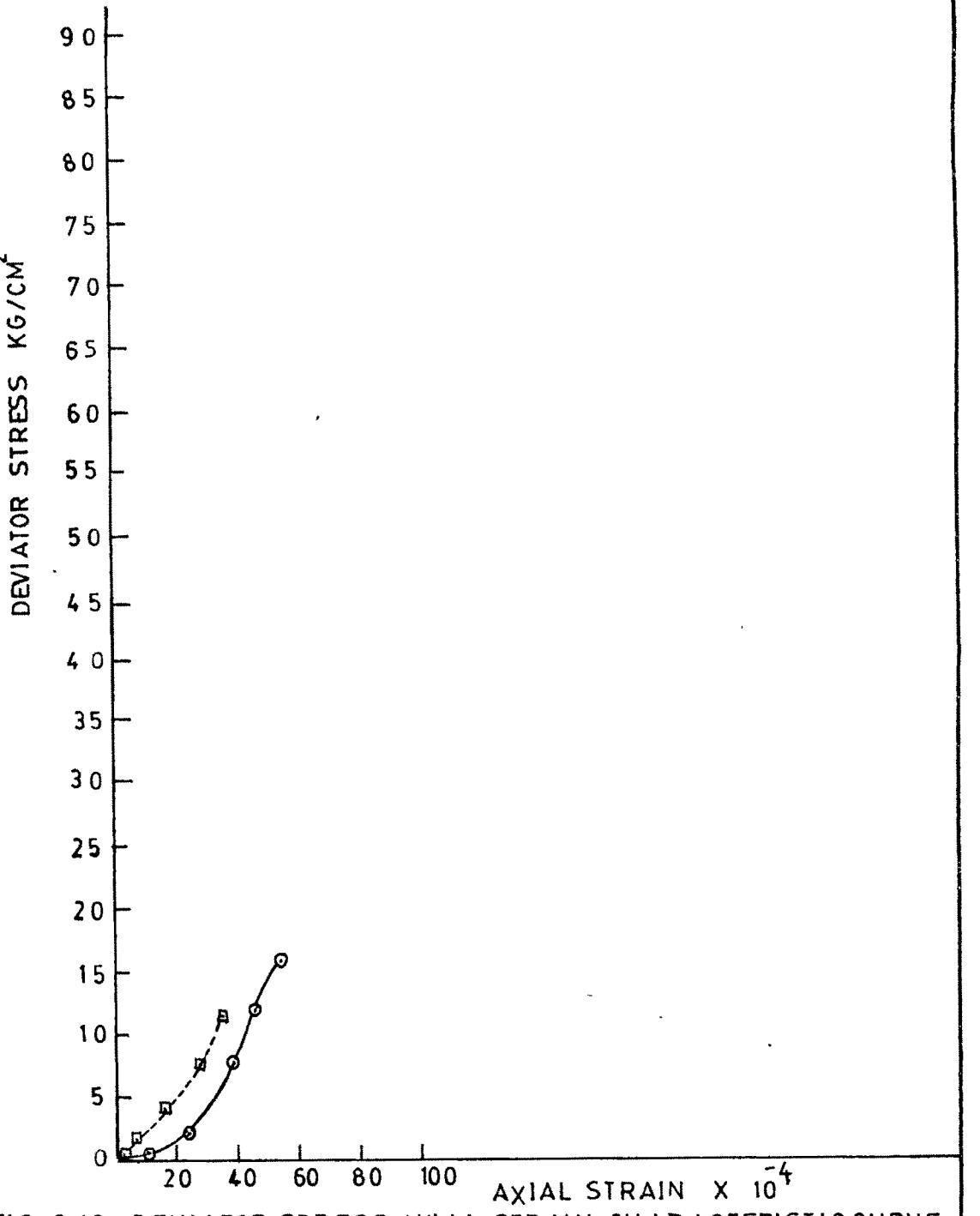

FIG. 6·42 DEVIATOR STRESS AXIAL STRAIN CHARACTERISTIC CURVE

	DESIGNATION	DEVIATOR STRESS AT FAILURE kg/cm^2	STRESS RATIO AT FAILURE $\frac{\sigma_1}{\sigma_3}$	AXIAL STRAIN AT FAILURE 10^{-4}
———	$39/Z_8^{54\cdot8}$	18·86	3·38	36·42
– – –	$51/ZZ_8^{54\cdot8}$	43·50	6·44	32·08

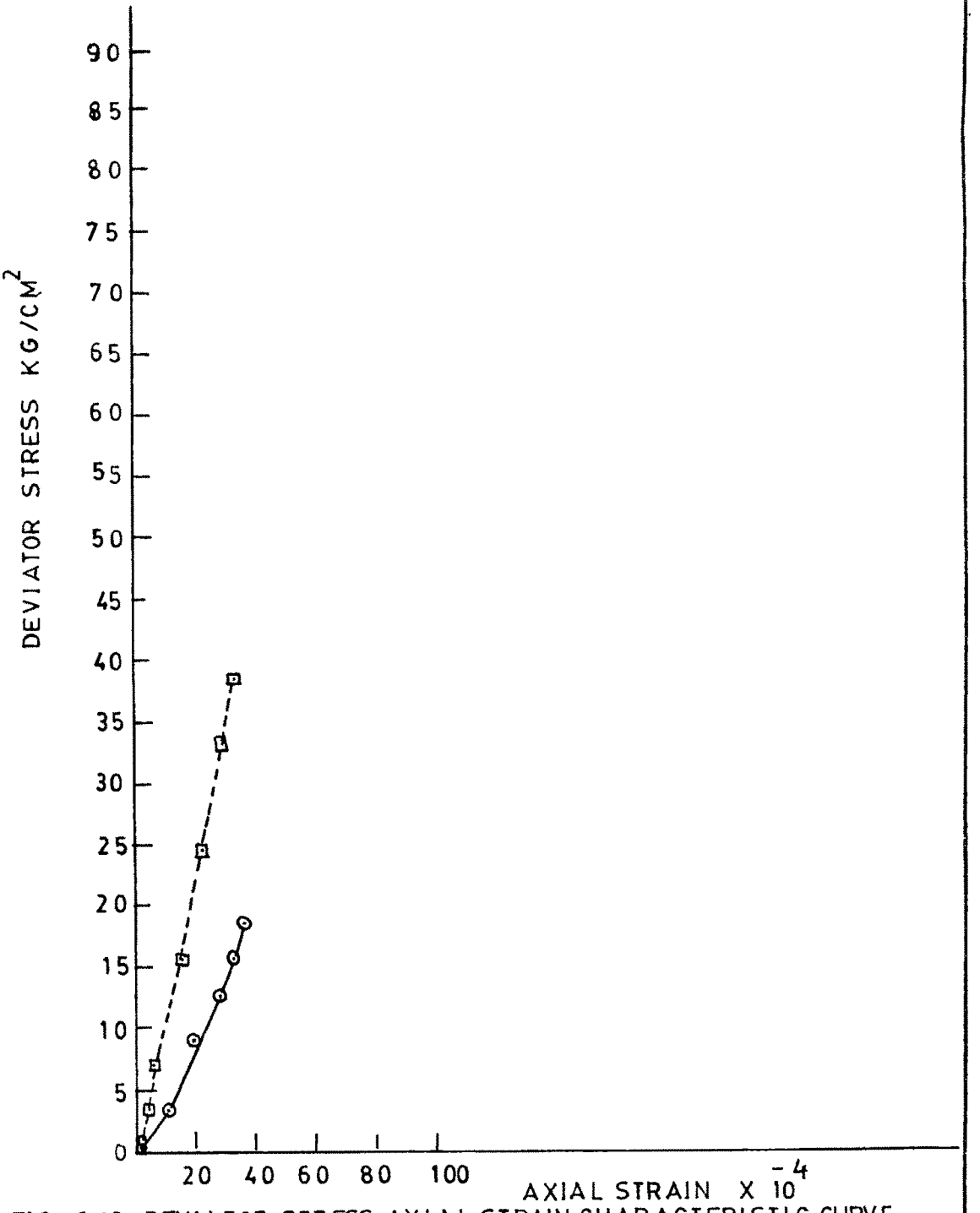

FIG. 6-43 DEVIATOR STRESS AXIAL STRAIN CHARACTERISTIC CURVE

materials (cement:bentonite 50:50, 40:60 and 30:70), for two different sizes (N_x and A_x) and at 2 kg/cm^2, 4 kg/cm^2, 6 kg/cm^2 and 8 kg/cm^2 cell pressures respectively. Though the nature of the stress-strain curves are similar there appears prominant changes in the corresponding stress values indicating that the modulii gets reduced as the size increases. The degree of downward concavity appears to increase with the size of the samples. It is observed that the values of stress-ratio do not change significantly with the size of the specimen, though the stress strain curves differ in trajectory indicating that the failure may occur almost at the same stress combination but the stress-strain relationship may not be identical.

6.4.4 Catagory - IV

6.4.4.1 Monotonic loading

Figures 6.44 to 6.48 are graphic representations of stress-strain and volume change characteritics of samples tested employing closed loop servo controlled MTS set up under monotonic loading. Figures 6.44 to 6.46 show the stress strain and volume change characteristic curves for samples with gouge as cement:sand 1:3 joint orientation 45° to the horizontal and at cell pressures 2 kg/cm^2, 4 kg/cm^2 and 6 kg/cm^2 respectively. Figures 6.47 and 6.48 show the stress strain and volume change charateristic curves for samples with gouge as cement:sand 1:3, at cell pressure 4 kg/cm^2 and at joint orientations 54.8° and 30° to the horizontal respectively. The stress strain curves obtained employing closed loop servo controlled MTS set up reveal similar characteristic

DESIGNATION	DEVIATOR STRESS AT FAILURE Kg/cm^2	STRESS RATIO AT FAILURE σ_1/σ_3	AXIAL STRAIN AT FAILURE 10^{-4}	DILATANCY $\left(1-\frac{d(\frac{\Delta v}{v})}{d\epsilon_1}\right)$
B_2^{45} *	8·94	5·47	7·19	0·606

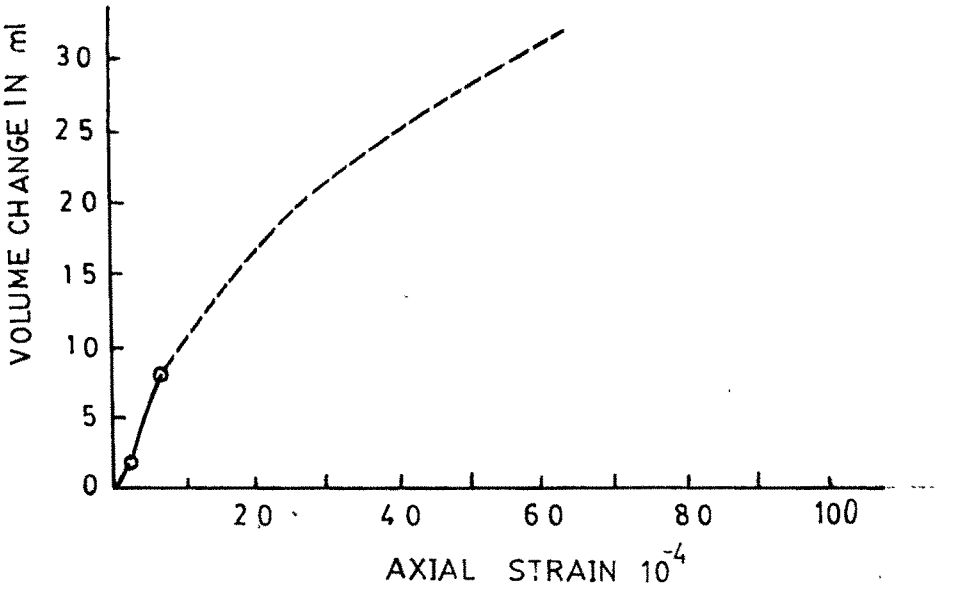

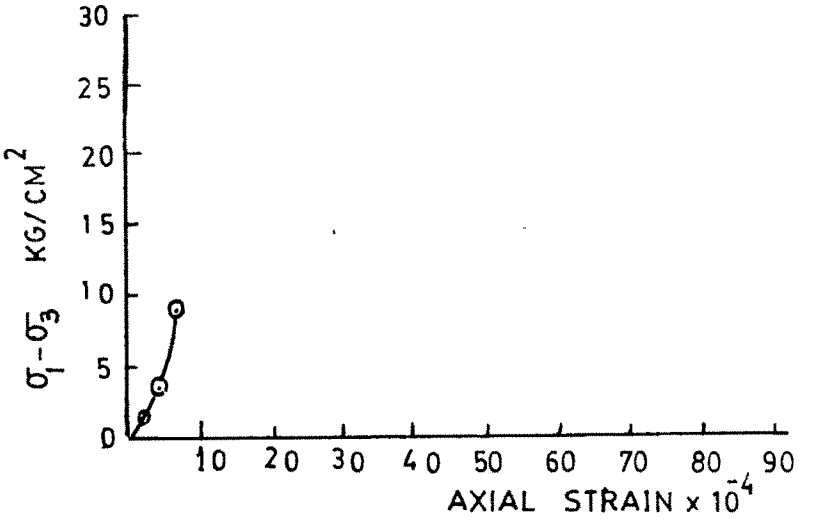

FIG.6·44 DEVIATOR STRESS AXIAL STRAIN VOLUME CHANGE CHARACTERISTIC CURVE

DESIGNATION	DEVIATOR STRESS AT FAILURE Kg/cm²	STRESS RATIO AT FAILURE σ_1/σ_3	AXIAL STRAIN AT FAILURE 10^{-4}	DILATANCY $\left(1-\frac{d(\frac{\Delta V}{V})}{d\epsilon_1}\right)$
B_4^{45} *	14 02	4·51	10·00	0·631

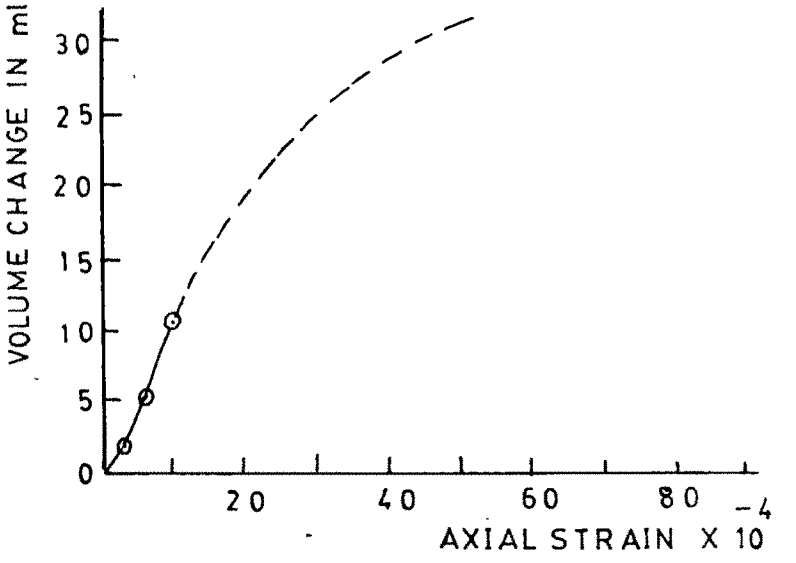

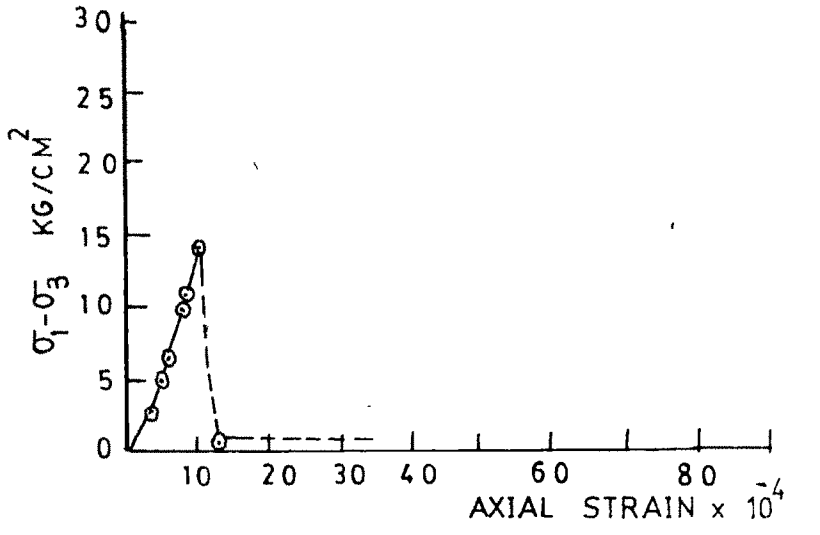

FIG.6·45 DEVIATOR STRESS AXIAL STRAIN VOLUME CHANGE CHARACTERISTIC CURVE

DESIGNATION	DEVIATOR STRESS AT FAILURE Kg/cm²	STRESS RATIO AT FAILURE σ_1/σ_3	AXIAL STRAIN AT FAILURE 10^{-4}	DILATANCY $\left(1-\frac{d(\frac{\Delta V}{V})}{d\epsilon_1}\right)$
B_6^{45*}	34·38	6·73	50·00	0·604

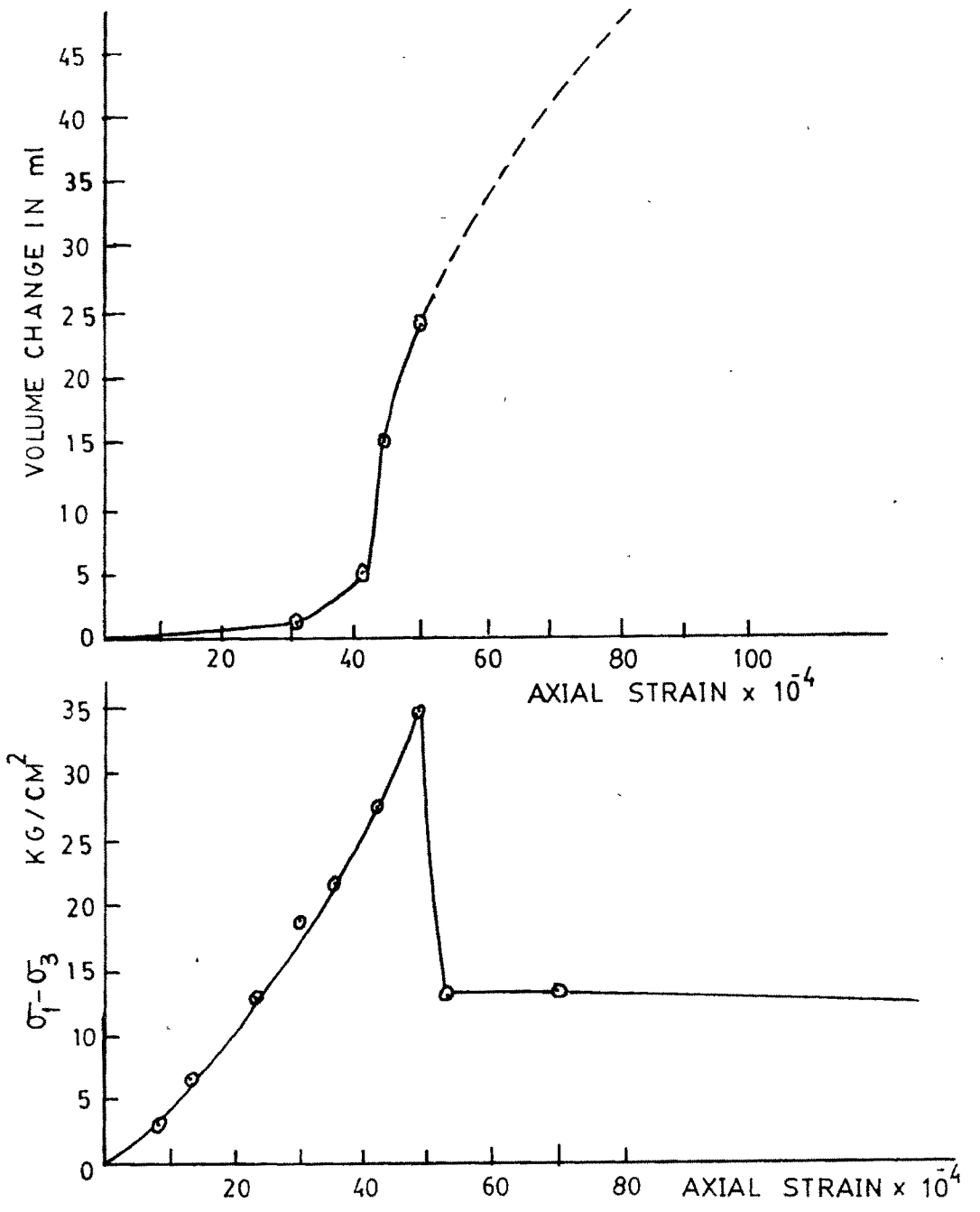

FIG.6·46 DEVIATOR STRESS AXIAL STRAIN VOLUME CHANGE CHARACTERISTIC CURVE

DESIGNATION	DEVIATOR STRESS AT FAILURE Kg/cm^2	STRESS RATIO AT FAILURE σ_1/σ_3	AXIAL STRAIN AT FAILURE 10^{-4}	DILATANCY $\left(1-\frac{d(\frac{\Delta V}{V})}{d\epsilon_1}\right)$
$B_4^{54\cdot8*}$	28·15	8·04	12·30	0·848

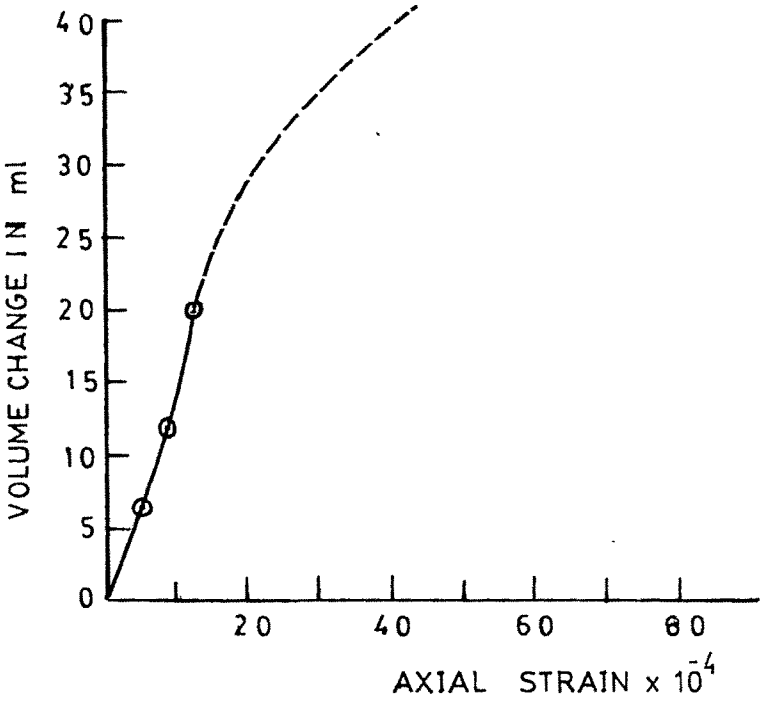

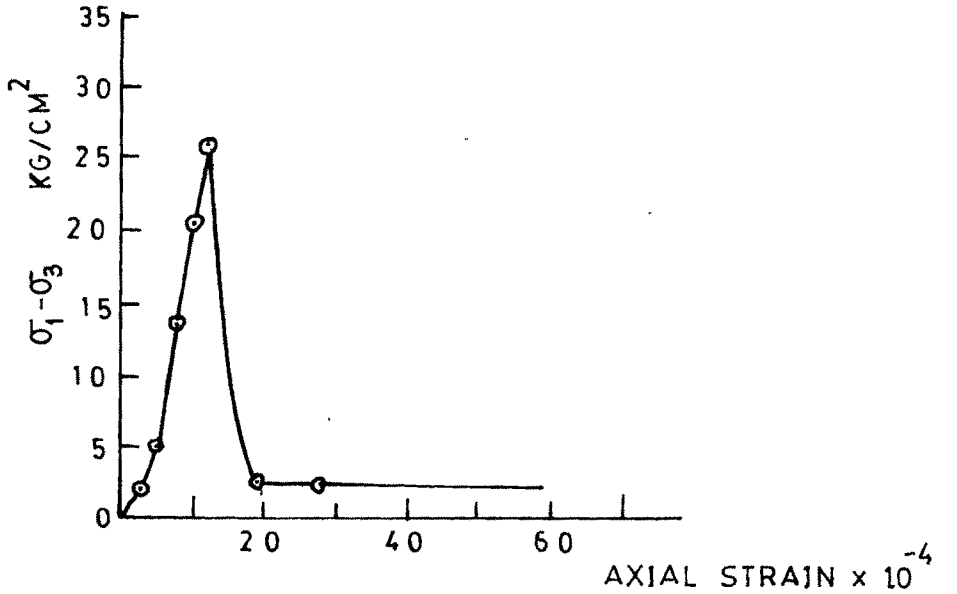

FIG.6·47 DEVIATOR STRESS AXIAL STRAIN VOLUME CHANGE CHARACTERISTIC CURVE

DESIGNATION	DEVIATOR STRESS AT FAILURE Kg/cm^2	STRESS RATIO AT FAILURE σ_1/σ_3	AXIAL STRAIN AT FAILURE 10^{-4}	DILATANCY $\left(1-\frac{d(\frac{\Delta V}{V})}{d\epsilon_1}\right)$
B_4^{30}	171·61	43·90	106·17	0·967

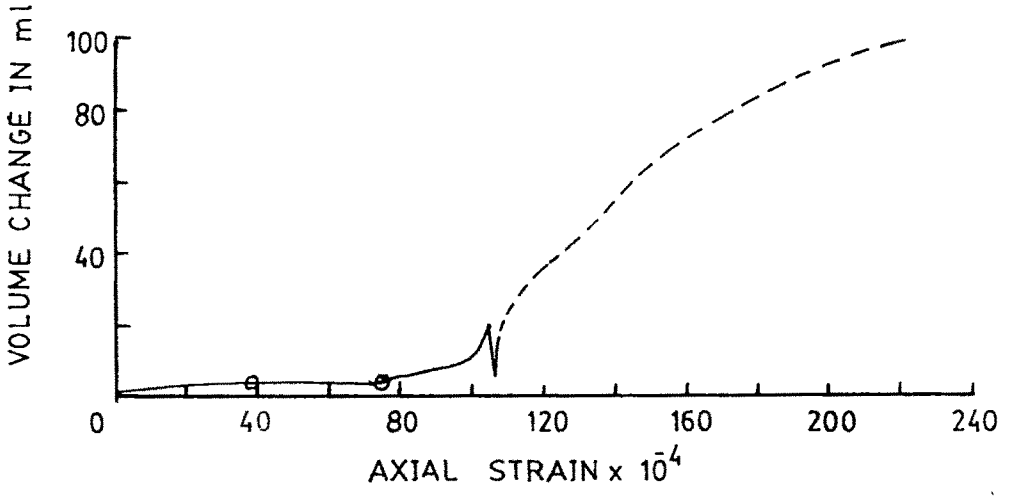

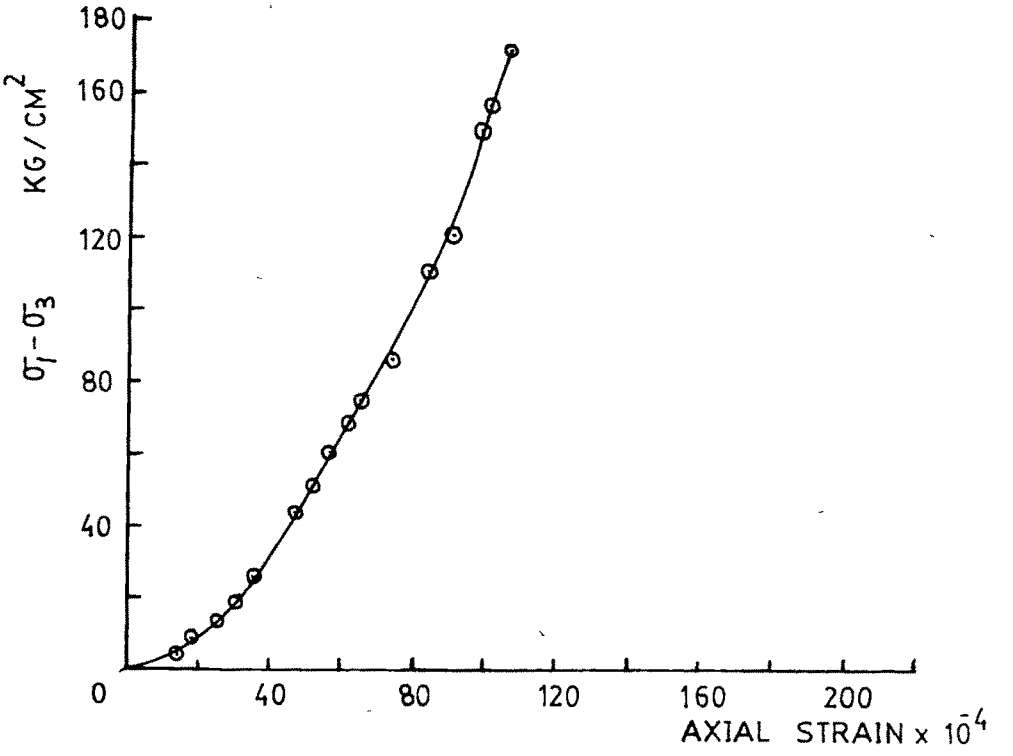

FIG. 6·48 DEVIATOR STRESS AXIAL STRAIN VOLUME CHANGE CHARACTERISTIC CURVE

curves depicting concave downward in the early stages of loading to those observed using conventional strain controlled triaxial setup. The volume of water out flowing from the cell was observed during the test for understanding the volume change characteristics. The volume of water out flow appears to conform with the probable volume change characteristics, initially the volume of water outflow is very low and slightly increases till peak but just near and or after peak stress the volume of water out flow show phenomenal increase. The post peak behaviour also could be observed in the test conducted through closed loop servo controlled MTS setup. It is seen that after the peak there occurs a sudden drop with characteristic thud noise and then stabilizes at constant stress value. This characteristic is predominantly observed in cases of specimens with joint orientations of 30° and 45°.

6.4.4.2 Triangular loading

Figure 6.49 shows graphically stress strain curve for the specimen with gouge material as cement : sand 1:3, joint orientation 54.8° with horizontal and at 4 kg/cm^2 cell pressure tested in closed loop servo controlled MTS setup under triangular loading cycles. The event consisted of employing two consecutive cycles at particular load level and then the load level is increased and further two consecutive cycles are employed in which manner the sequence is followed upto failure. It can be observed clearly that the concave downward nature in the initial stage of loading is present persistantly. At unloading the hysterisis loop is

DESIGNATION	DEVIATOR STRESS AT FAILURE kg/cm^2	STRESS RATIO AT FAIURE σ_1/σ_3	AXIAL STRAIN AT FAILURE 10^{-4}	DILATANCY $\left(1-\frac{d(\frac{\Delta V}{V})}{d\epsilon_1}\right)$
$B_4^{54\cdot8}$	23·32	6·83	17·1	0·896

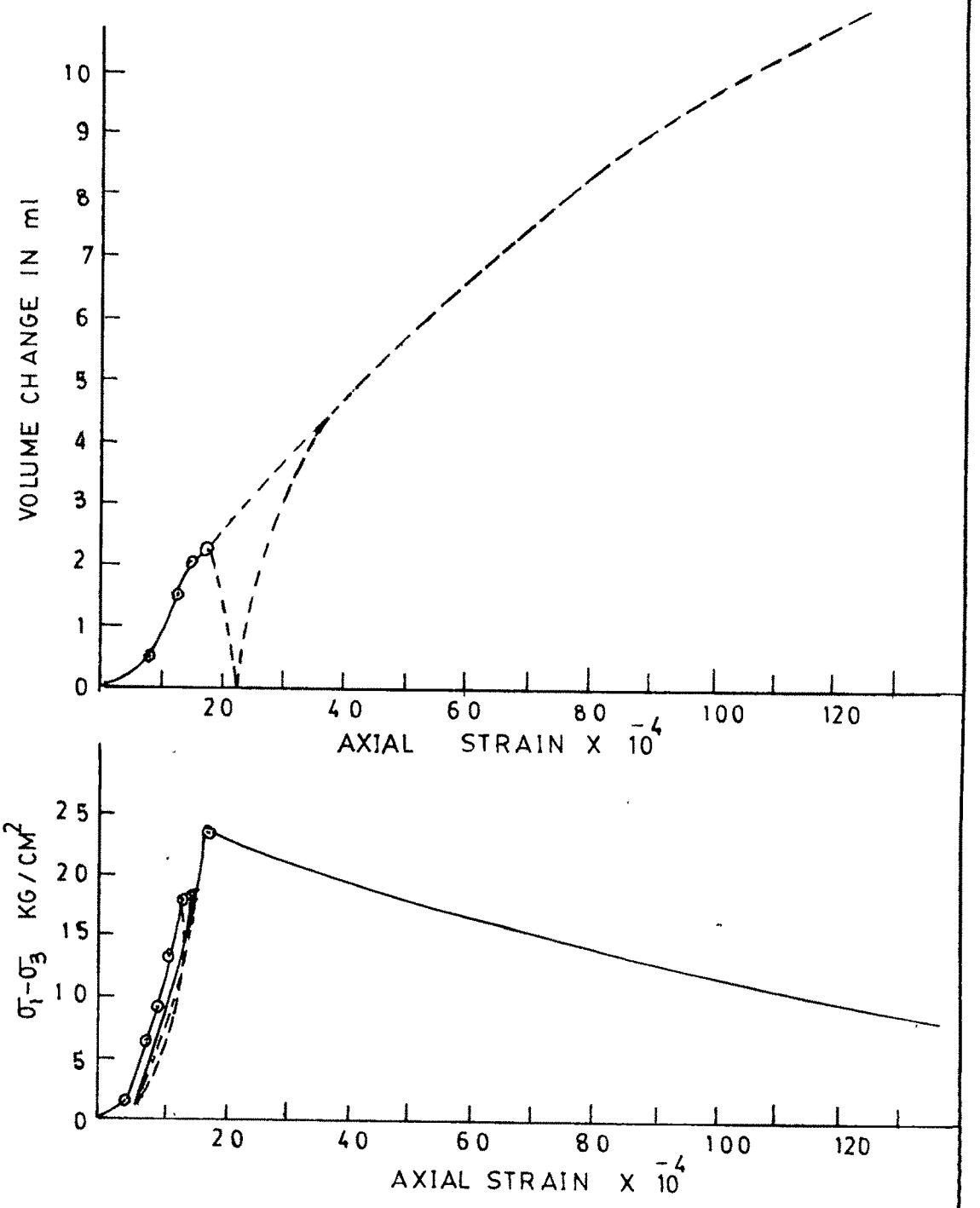

FIG. 6-49 DEVIATOR STRESS AXIAL STRAIN VOLUME CHANGE CHARACTERISTIC CURVE

clearly observed which appears to remain almost constant during the repeated cycle of loading. The volume of water outflow is negligible in the prepeak region and only near or after the peak there is phenomenal volume of water outflow. It was also observed a sudden drop in volume of water out flow just at the peak but it immediately picks up and follows the characteristics. This may be attributed to the quick reversal of stresses.

6.4.4.3 Sinusoidal loading

Figure 6.50 shows graphically stress-strain and volume change characteristic curves for the specimen with gouge material as cement : sand 1:3 joint orientation 54.8° with horizontal and at 4 kg/cm^2 cell pressure tested in closed loop servo controlled MTS setup under sinusoidal loading for two consecutive cycles and then the load is increased and further two consecutive cycles are given and the sequence is followed till failure. In sinusoidal loading event also the similar concave downward nature in the initial stages is observed as in triangular loading event. During the loading and unloading cycles the hysterisis loop is clearly observed which appears to remain almost constant during consecutivly repeated cycles. In this case also the volume of water outflow is negligible in the prepeak region and only near or after the peak there is phenomenal volume of outflow. It was also observed a sudden drop in volume of water outflow just at peak but it immediately picks up and follows the characteristic. This characteristic is noticed only in both the triangular cyclic loading event and sinusoidal cyclic

DESIGNATION	DEVIATOR STRESS AT FAILURE kg/cm^2	STRESS RATIO AT FAILURE σ_1/σ_3	AXIAL STRAIN AT FAILURE 10^{-4}	DILATANCY $\left(1-\frac{d(\frac{\Delta V}{V})}{d\epsilon_1}\right)$
$B_4^{54\cdot8***}$	75·18	19·80	66·50	0·865

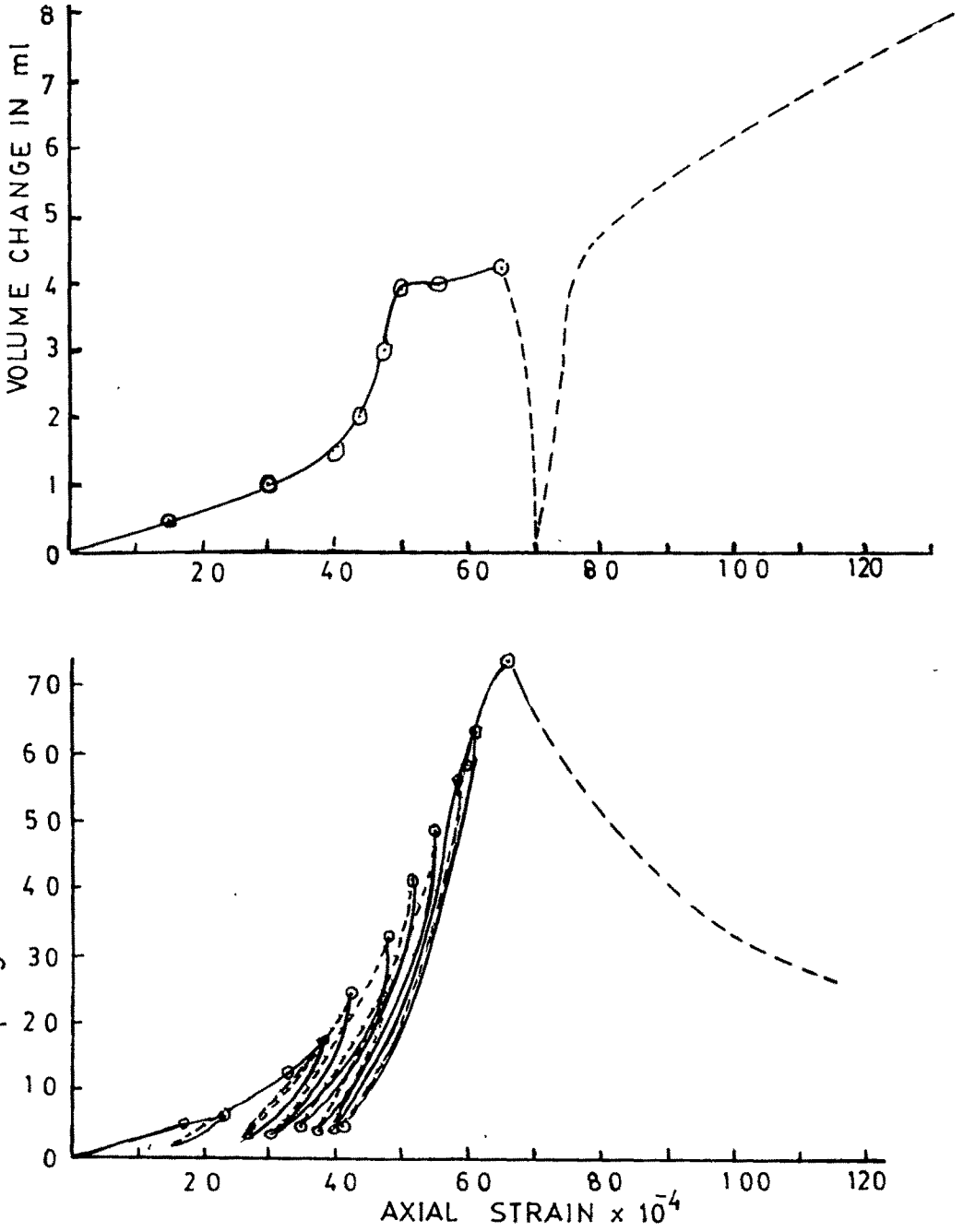

FIG. 6·50 DEVIATOR STRESS AXIAL STRAIN VOLUME CHANGE CHARACTERISTIC CURVE

loading event. This characteristic may be attributed to the quick reversal of stresses.

6.5.0. CONCLUDING REMARKS

Experimental investigations were conducted to study the various factors affecting the shearing behaviour of jointed rocks under the theoretical background developed in the previous chapter. It was possible to prepare the samples of jointed rocks in the laboratory with the aid of specially developed grips and modified conventional process for filling in the gouge materials under the controlled conditions. The conventional strain controlled test setup has successfully been employed for obtaining the data for the analysis. Special tests were attempted on closed loop servo controlled MTS set up with a view to investigate closely and compare the observations with conventional test setup. The tests on MTS has furnished valuable observations in the post peak zones and also the volumatric changes during the process of deformation. These observations should provide the data for the analysis and conclusions on the important fundamental aspects as regard shearing behaviour of jointed rocks.